Computers & Geosciences 196 (2025) 105821

Contents lists available at ScienceDirect

Computers and Geosciences

journal homepage: www.elsevier.com/locate/cageo

Quantitative lithology prediction from seismic data using deep learning

Wenliang Nie [a,b,*], Jiayi Gu [a], Bo Li [c], Xiaotao Wen [c], Xiangfei Nie [a]

[a] School of Electronic and Information Engineering, Chongqing Three Gorges University, Chongqing, 404000, China
[b] State Key Laboratory of Oil and Gas Reservoir Geology and Exploitation, Chengdu University of Technology, Chengdu, 610059, China
[c] School of Geophysics, Chengdu University of Technology, Chengdu, 610059, China

ARTICLE INFO

Keywords:
Quantitative lithology prediction
AdaBoost-CNN
Non-convex L1−2 regularization
Unbalanced dataset

ABSTRACT

Lithology prediction is essential for understanding subsurface structures and properties. Deep learning (DL) methods, which can capture the nonlinear relationship between lithology and seismic data, have gained significant attention as an effective tool in lithology prediction. However, these methods still face many challenges such as limited well-log data, class imbalances, and the need for robust predictive models. To address these issues, we propose an adaptive boosting-convolutional neural network (AdaBoost-CNN) framework integrated with improved inverse spectral decomposition (ISD) based on non-convex $L_{1\text{-}2}$ regularization. The ISD method generates high-resolution time-frequency (T-F) spectral maps from seismic data, which serve as inputs for the CNN. Furthermore, we introduce an enhanced sample weight adjustment strategy and a "CNN transfer" mechanism within the AdaBoost framework to address class imbalance and enhance training efficiency. The performance of AdaBoost–CNN was validated through field cases, and a comprehensive evaluation of the model parameters was conducted to understand their impact on performance. Field experiments demonstrated that the proposed method enhanced both the training efficiency and generalization ability of the models. Additionally, it effectively predicted lithology from seismic data and quantified lithology probabilities, thereby providing insights into the distribution of subsurface lithology.

1. Introduction

Lithology prediction is a complex process in seismic exploration, aiming to infer subsurface properties from seismic data (Adler et al., 2021; Yu and Ma, 2021). However, this task is inherently challenging owing to two primary factors: (1) the ambiguity introduced by different rock types yielding similar seismic responses, and (2) the low vertical resolution of seismic data, which limits the ability to accurately delineate subsurface features (Pan et al., 2023). The most commonly used approaches for lithology prediction are traditional and data-driven methods. Traditional methods, such as linearized amplitude variation with offset (AVO) inversion, Bayesian AVO inversion, and Markov Chain Monte Carlo (MCMC) methods, establish nonlinear relationships between seismic data and subsurface structures to estimate elastic properties like P-wave and S-wave impedances (Fig. 1(a)) (Adler et al., 2021; Bosch et al., 2010; Nie et al., 2021). Then, using these data, the relationships between these parameters and lithology are calculated and analyzed to infer the lithology of subsurface rock layers. However, these methods may introduce uncertainty or reduce the precision of lithology prediction because of the approximation of nonlinear relationships and ill-posed inverse problems (Grana et al., 2022). Conventional data-driven methods use lithology-sensitive parameters extracted from well-logging and seismic data to characterize seismic lithology or reservoirs, such as cross-plot analysis (Okeugo et al., 2019), pattern recognition (Sahoo and Jha, 2017), and cluster analysis identification (Kitzig et al., 2017). However, based on post- or pre-stack inversion results, such as P-, and S-waves, and density, lithology probability can be predicted using machine-learning methods or Bayesian classification (Karakaya et al., 2024). These methods rely on a large number of samples, which is difficult to achieve in seismic exploration, and are time-consuming(Lin et al., 2020; Singh et al., 2020; Zeng et al., 2022).

In recent years, deep learning (DL) has become increasingly prominent in seismic lithology and reservoir prediction owing to its ability to perform nonlinear mapping approximations and provide uncertainty projections, particularly for seismic facies analysis (Feng et al., 2021; Miele and Azevedo, 2024), and lithology prediction (Li et al., 2018; Zeng et al., 2020). Convolutional neural networks (CNNs) can be used to predict lithology directly, demonstrating superior performance in DL feature extraction and hierarchical pattern recognition (Alzubaidi et al., 2021; Imamverdiyev et al., 2019). CNNs can extract features from

* Corresponding author. School of Electronic and Information Engineering, Chongqing Three Gorges University, Chongqing, 404000, China
E-mail address: niewenliang@sanxiau.edu.cn (W. Nie).

https://doi.org/10.1016/j.cageo.2024.105821
Received 1 July 2024; Received in revised form 10 December 2024; Accepted 10 December 2024
Available online 12 December 2024
0098-3004/© 2024 Elsevier Ltd. All rights are reserved, including those for text and data mining, AI training, and similar technologies.

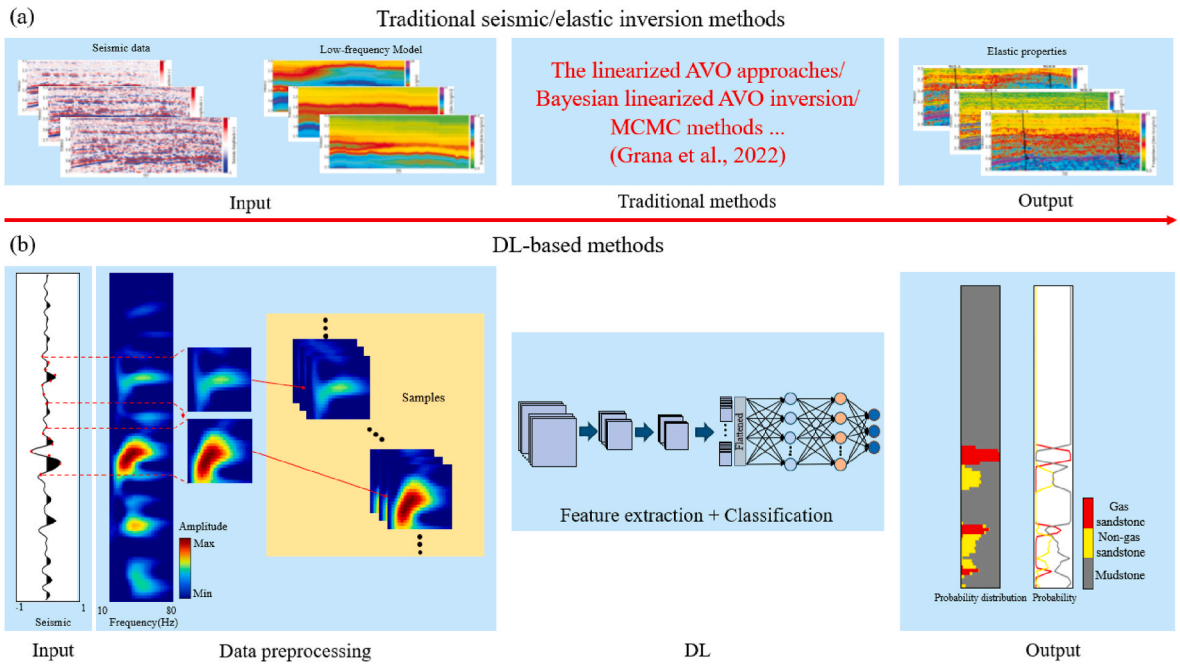

Fig. 1. A comparison between traditional inversion approaches and DL-based methods.

various data formats, including 2-dimensional (2-D) and 3-dimensional images, and 1-dimensional (1-D) vector signals (Li et al., 2020; Wu et al., 2020). This feature makes CNNs particularly effective in tackling complex geological problems (Liu et al., 2020; Wu et al., 2019). Time-frequency (T-F) analysis is a useful tool for generating multiscale attributes for lithology prediction, as it can directly extract features that are difficult to identify through traditional time-domain analysis (Bauer et al., 2020; Li et al., 2019). Considering the non-stationary characteristics of seismic data, abrupt changes or abnormal reflections appear as specific textures and shapes in the T-F spectrum (Ali et al., 2022; Liu et al., 2022). These results, when used as input samples for DL, can effectively improve lithology prediction accuracy. Continuous wavelet transform (CWT)-CNN was proposed by combining the CWT and CNN, which can directly use the T-F spectrum of seismic data to predict seismic lithology and reservoirs (Zhang et al., 2018). Subsequently, a modified T-F analysis tool and a CNN were used to improve the accuracy of the results of lithology prediction (Zeng et al., 2020a, b).

However, existing DL-based methods face several challenges (Grana et al., 2020). First, conventional T-F analysis tools have often been used in combination with the DL method for seismic lithology prediction, failing to fully exploit the frequency information of noisy seismic data, resulting in limited prediction accuracy and resolution (Zhang et al., 2018, 2020). Second, gas or oil is typically found within porous and permeable rock formations or interspersed within the reservoir rock. These reservoirs are collected from in the small interconnected pore spaces of the rock and are confined by adjacent and overlying impermeable rock layers. This situation presents a challenge in DL, where reservoir classes are typically underrepresented, whereas non-reservoir classes dominate the data. DL models are prone to overfitting when dealing with class imbalances, which compromises model robustness and leads to local optima convergence during training (Zhu et al., 2019). Finally, unlike other fields, training data is often incomplete due to high drilling costs and the minimal well-logging data. This further limits the generalization ability of models under supervised learning, potentially leading to high misidentification rates during lithological predictions (Taherkhani et al., 2020).

To address these issues, we propose a novel deep learning-based approach that combines improved inverse spectral decomposition (ISD) with an adaptive boosting convolutional neural network (AdaBoost-CNN) (Fig. 1(b)). AdaBoost, as an ensemble method, is well-suited for handling imbalanced datasets through iterative weight adjustments that focus on difficult-to-classify samples. CNNs, however, excel at feature extraction from seismic data, making them powerful tools for identifying hierarchical and spatial structures (Maged and Xie, 2023). However, directly applying the standard AdaBoost to CNNs introduces computational inefficiencies owing to the large parameter space of deep networks. To overcome this limitation, we introduced a CNN transfer, a strategy that enables the transfer of learned model weights (convolutional and fully connected layer parameters) between successive CNN estimators in the AdaBoost framework. This innovation significantly reduced the computational costs while maintaining high prediction accuracy. The main contributions of this study are as follows.

- The T-F analysis was improved using non-convex $L_{1\text{-}2}$ regularization on inverse spectral decomposition (ISD), resulting in high-resolution input data for the DL models.
- We introduce a "CNN transfer" mechanism—that allows base estimators within the AdaBoost framework to inherit model weights from previous iterations. This strategy improves training efficiency and convergence speed.
- The proposed method of combining ISD with AdaBoost-CNN provides quantitative probability results for seismic lithology predictions.

This study is organized as follows: the proposed ISD and AdaBoost-CNN architecture details are presented in Section 2. In Section 3, the proposed method is applied to a field test, and the results of comparative tests are verified. Finally, the discussion and conclusion are presented in Section 4 and Section 5, respectively.

2. Proposed methodology

2.1. Non-convex L_{1-2} regularization for ISD

The recorded seismic data $s(t)$ can be represented in the convolutional form of seismic wavelets with different dominant frequencies and reflection coefficients (Bonar and Sacchi, 2010), as follows:

$$s(t) = \sum_{m=1}^{M} [w(t,f_m)*r(t,f_m)] + n(t) \tag{1}$$

where $n(t)$ is the noise, t is the sample time, $m = [1, 2, \ldots, M]$, M represents the total number of wavelets with dominant frequency f_m, $w(t,f_m)$ represents the complex wavelets with frequency f_m, and $r(t,f_m)$ represent the complex reflection coefficients, which include the frequency and phase information of the wavelets.

We rewrite Eq. (1) in matrix form as follows:

$$\boldsymbol{s} = \boldsymbol{Gm} + \boldsymbol{n} = [\boldsymbol{W}_1 \quad \boldsymbol{W}_2 \quad \cdots \quad \boldsymbol{W}_M] \begin{bmatrix} \boldsymbol{r}_1 \\ \boldsymbol{r}_2 \\ \vdots \\ \boldsymbol{r}_M \end{bmatrix} + \boldsymbol{n} \tag{2}$$

where $\boldsymbol{s}$ is the seismic data vector, $\boldsymbol{s} = [s_1, s_2, \ldots, s_N]$, N is the max sample length, $\boldsymbol{G} \in \boldsymbol{R}^{N\times MN}$ is the wavelets kernel matrix, $\boldsymbol{m} \in \boldsymbol{R}^{MN\times 1}$ is the series of reflection coefficients composed of $\boldsymbol{r}_M$. $\boldsymbol{n}$ is the noise vector. $\boldsymbol{W}_M \in \mathbf{R}^{N\times N}$ is the wavelet kernel matrix with dominant frequency f_m, $\boldsymbol{r}_M \in \mathbf{R}^{N\times 1}$ are the reflection coefficients. The $\boldsymbol{r}_M$ value is the weight of the corresponding wavelet with frequency f_m in the seismic data. By reshaping the $\boldsymbol{m}$ values, we obtained a T-F spectral map of the seismic data. Eq. (2) is an ill-posed issue in that $\boldsymbol{G}$ is a sensing matrix ($NM \gg N$). Although some existing L_1 regularization-based methods have been applied to solve this problem, it was proved that non-convex L_{1-2} regularization has better performance than that of L_1 regularization (Yin et al., 2015). Moreover, non-convex L_{1-2} regularization has been developed in geophysics fields, such as seismic inversion (Nie et al., 2020), and seismic attenuation compensation (Wang et al., 2018, 2022). Hence, we introduced the following method to solve this problem:

$$\min_m \frac{1}{2}\|\boldsymbol{Gm} - \boldsymbol{s}\|_2^2 + \lambda(\|\boldsymbol{m}\|_1 - \alpha\|\boldsymbol{m}\|_2) \tag{3}$$

where λ is a regularization parameter, and α is a weight parameter, with range [0, 1].

2.2. The AdaBoost-CNN algorithm

The AdaBoost algorithm (Freund et al., 1997), is a popular ensemble learning method that combines multiple weak classifiers to construct a strong classifier with improved accuracy. The central idea of AdaBoost is to sequentially train a series of base classifiers, where each subsequent classifier focuses on the errors made by its predecessor. This iterative process effectively enhances the performance of the overall model by forcing the base learners to specialize in different aspects of the data.

In this study, we employed the multi-class AdaBoost technique (Hastie et al., 2009) to integrate multiple CNNs into a single ensemble model, which we refer to as AdaBoost-CNN. This method incorporates model weight transfer for CNN estimators and updates the sample weights based on the cross-entropy error. The training set used during the training process was defined as:

$$\{(\boldsymbol{x}_1, \boldsymbol{y}_1), (\boldsymbol{x}_2, \boldsymbol{y}_2), \ldots, (\boldsymbol{x}_N, \boldsymbol{y}_N)\} \tag{4}$$

where $\boldsymbol{x}_i$ represents the input sample, and $\boldsymbol{y}_i$ is the output corresponding to $\boldsymbol{x}_i$, represented as a probability distribution over K classes, that is, $\boldsymbol{y}_i \in \Delta^{K-1}$. Here, Δ^{K-1} denotes the (K-1)-simplex, defined as:

$$\Delta^{K-1} = \left\{ \boldsymbol{y} \in R^K : y_k \geq 0, \sum_{k=1}^{K} y_k = 1 \right\} \tag{5}$$

where $\boldsymbol{y}_k$ is the probability of $\boldsymbol{x}_i$ belonging to class k, and K is the total

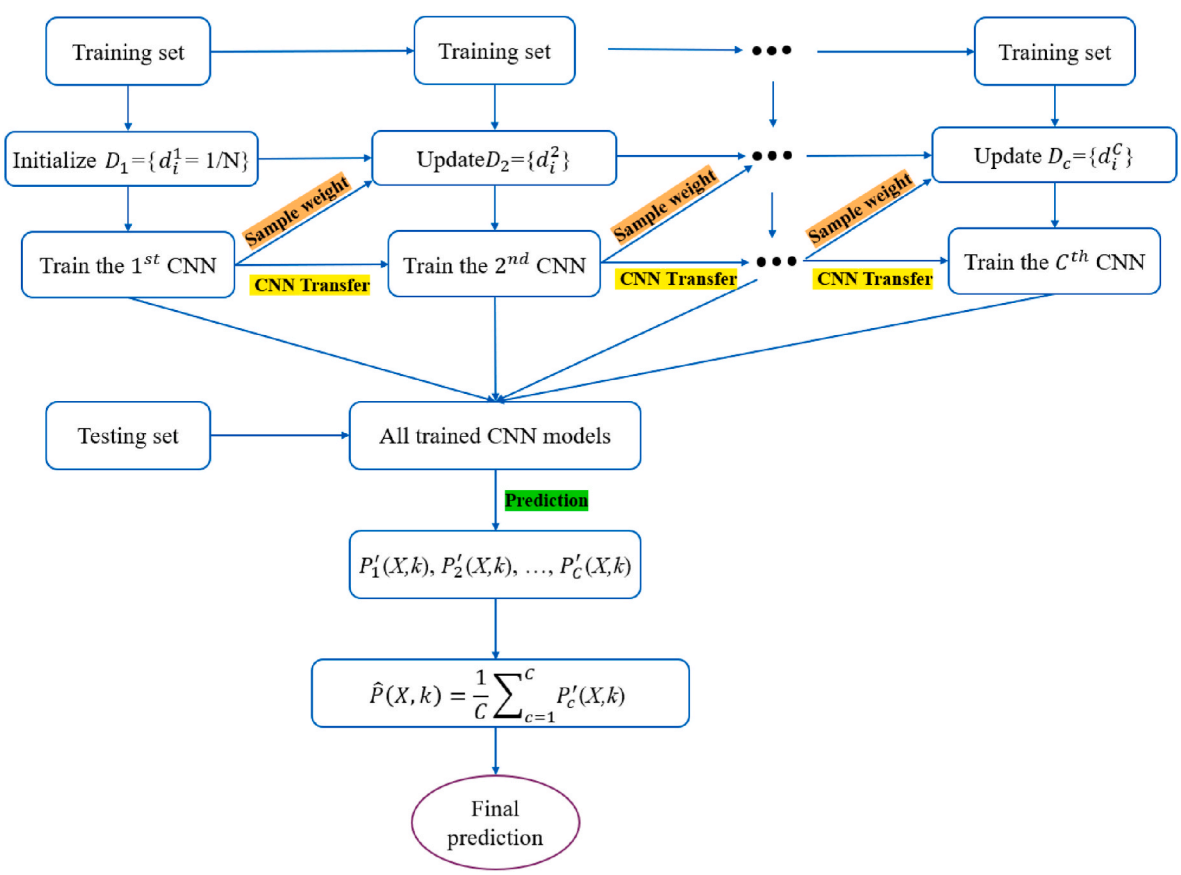

Fig. 2. AdaBoost-CNN method schematic.

number of classes.

Initially, all elements were assigned equal weights $d_i = 1/N$. For subsequent training rounds, the CNN used a weight initialization strategy that began with random weights and subsequently adopted the weights trained in the previous CNN as the starting point. After training, each CNN outputs a K-dimensional probability vector, as follows:

$$\boldsymbol{P}(\boldsymbol{x}_i) = [p_k(\boldsymbol{x}_i)], k = 1, \ldots, K \tag{6}$$

where $p_k(\boldsymbol{x}_i)$ indicates the probability that the input sample is in class k, and K refers to the total number of categories.

The sample weight d_i^{c+1} was updated after the cth iteration based on the classification result $\boldsymbol{P}(\boldsymbol{x}_i)$ of the CNN on the training set. This was specifically expressed as follows:

$$d_i^{c+1} = d_i^c \cdot \exp\left(\alpha \cdot \left(-\sum_{k=1}^{K} \boldsymbol{y}_i \log(\boldsymbol{P}^c(\boldsymbol{x}_i))\right)\right), i = 1, \ldots, N \tag{7}$$

where d_i^c represents the weight of the ith sample used by the cth CNN, and α is the learning rate that controls the magnitude of weight updates. The term $-\sum_{k=1}^{K} \boldsymbol{y}_i \, log(\boldsymbol{P}^c(\boldsymbol{x}_i))$ is the cross-entropy error, where $\boldsymbol{y}_i$ and $\boldsymbol{P}^c(\boldsymbol{x}_i)$ denote the true distribution and predicted probability for the ith sample, respectively. The cross-entropy error measures the divergence between the true and predicted distributions of each sample. If the error is high (indicating prediction errors or low confidence), the sample weight d_i^{c+1} increases, making the sample more influential in the subsequent iteration. Conversely, if the error is low (indicating correct predictions with high confidence), the d_i^{c+1} weight decreases. To maintain total weight stability, the weights of all samples were normalized after each iteration.

Throughout the training, the CNN progressively enhanced the feature abstraction levels from simple textures to complex classes. Initially, convolutional layers used multiple filters to extract local features, such as edges and shapes. Common activations included ReLU and sigmoid functions. The pooling layer then downsized the feature map via downsampling (max pooling), thereby reducing the computational load while preserving essential information. These 2-D feature maps were flattened into 1-D vectors and fed into a fully connected layer that integrated all previous features for classification decisions. The output layer typically uses a softmax activation function to produce probability scores for each category. The CNN feature-extraction process and parameters setting is illustrated in Fig. 3.

To prevent overfitting, particularly in small dataset training scenarios (Hameed et al., 2020), subsequent iterations retained and optimized these weights, thereby enhancing CNN performance through weighted samples. After the C training iteration, all trained base estimators were tested on test sample $\widehat{\boldsymbol{x}}$.

The adjustment probability of a single basic estimator on the test set was calculated using Eq. (8),

$$\boldsymbol{P}_c{}'(\widehat{\boldsymbol{x}}) = (K-1)\left(\log(\boldsymbol{P}^c(\widehat{\boldsymbol{x}})) - \frac{1}{K}\sum_{k'=1}^{K} \log(\boldsymbol{P}_{k'}^c(\widehat{\boldsymbol{x}}))\right) \tag{8}$$

where k denotes a fixed class index for which the prediction probability is computed, whereas k' iterates over all classes to calculate the average probability across categories. The term $\log(\boldsymbol{P}^c(\widehat{\boldsymbol{x}}))$ represents the cth base estimator, which predicts the original probability that sample $\widehat{\boldsymbol{x}}$ belongs to category k. The term $\log(\boldsymbol{P}_{k'}^c(\widehat{\boldsymbol{x}}))$ represents the logarithm of the predicted probability for class k, where higher values indicate greater model confidence in classifying the sample as class k. The smoothing term $\frac{1}{K}\sum_{k'=1}^{K} \log(\boldsymbol{P}_{k'}^c(\widehat{\boldsymbol{x}}))$ averages the logarithmic probabilities across all categories, balancing the contributions between classes. This adjustment amplifies the impact of samples that are more challenging to classify, ensuring that the base estimators collectively focus on resolving classification difficulties.

The average of the adjusted probabilities $\boldsymbol{P}_c'(\widehat{\boldsymbol{x}})$ for all base estimators was calculated the final predicted probability:

$$\widehat{\boldsymbol{P}}_c(\widehat{\boldsymbol{x}}) = \frac{1}{C}\sum_{c=1}^{C} \boldsymbol{P}_c{}'(\widehat{\boldsymbol{x}}) \tag{9}$$

The detailed process of the proposed method is illustrated in (Fig. 2). Algorithm 1 provides the pseudo code for the proposed AdaBoost-CNN training method, with each step described in detail.

Algorithm 1. The proposed AdaBoost-CNN training method

Input: Training T-F maps and corresponding labels: $\{(\boldsymbol{x}_1, \boldsymbol{y}_1), (\boldsymbol{x}_2, \boldsymbol{y}_2), \ldots, (\boldsymbol{x}_N, \boldsymbol{y}_N)\}$

1. Weight d_i for each training data sample was set to $1/N$, where N represents the total number of training sets. The weights and error rates of the first CNN are initialized.

for c = 1 to C do

2. **if** c == 1 **then**

Train the first CNN using $\boldsymbol{D}^c = \{d_i^{c=1}\}$, $d_i^{c=1} = 1/N$;

else

Transfer the learning parameters of the previous CNN to the cth CNN;

Train the cth CNN on the training set using $\boldsymbol{D}^c = \{d_i^{c=1}\}$, which represents the current sample weights.

endif

3. Compute the cross-entropy error e_c of CNN on the training set;

4. **if** early stopping triggered or $e_c \geq 1 - 1/K$ **then**

Break the loop (K is the number of classes);

endif

5. The output $\boldsymbol{P}_c(\boldsymbol{x}_i)$ of CNN is used in Eq. (7) to update the sample weight d_i^{c+1};

6. Re-normalize the sample weights $\boldsymbol{D}^c = \{d_i^c\}$;

end for

Output: $\boldsymbol{P}_c(\boldsymbol{x}_i)$, which is the final predicted probability.

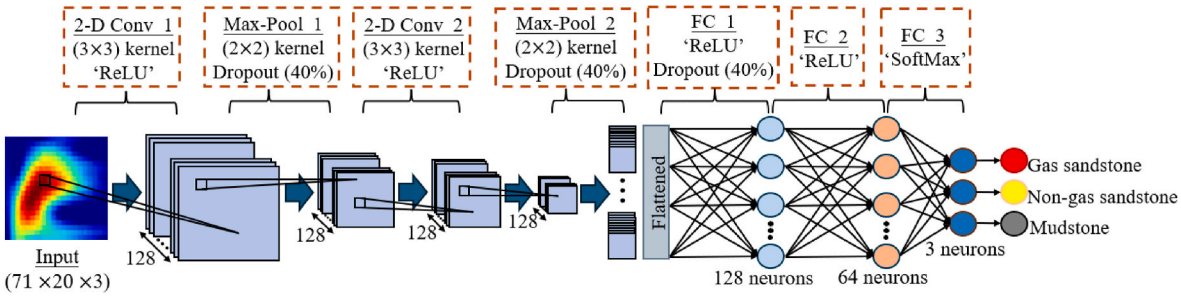

Fig. 3. CNN feature extraction.

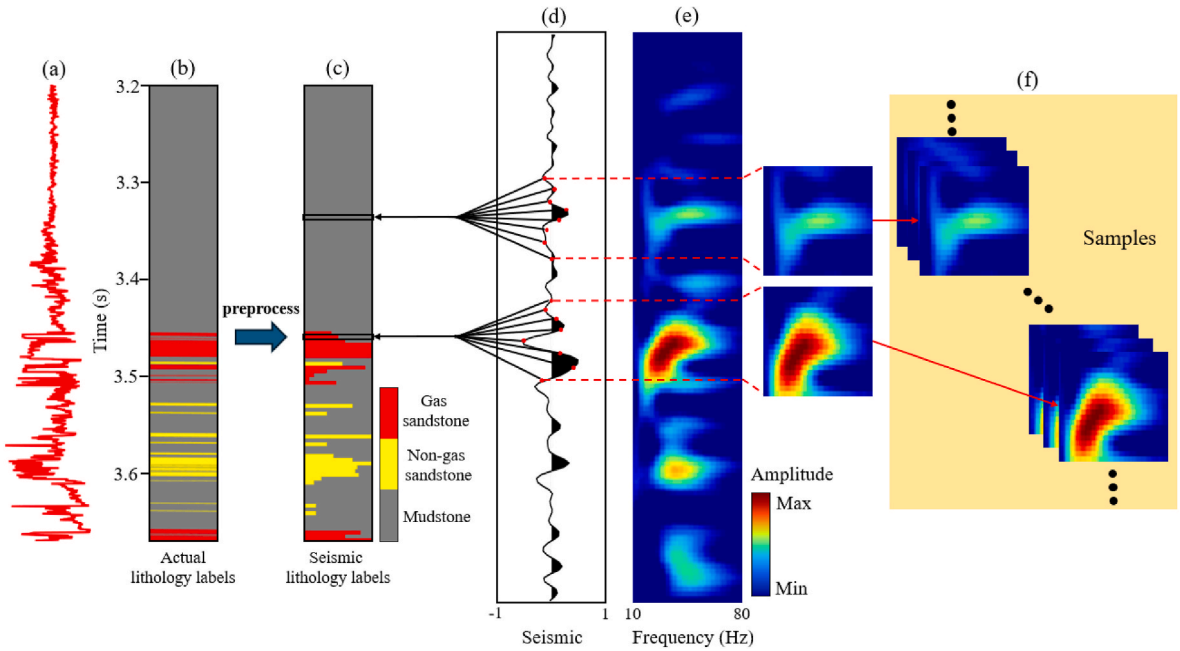

Fig. 4. The process of arranging post-stack seismic data into the CNN input samples; (a)–(d) display gamma-ray curves, actual and seismic lithology labels, and borehole-side seismic data, respectively; (e) shows the T-F spectrum using the proposed ISD method; and (f) presents the input samples for DL models.

2.3. Data preprocessing

Fig. 4 illustrates the technique for structuring post-stack seismic data into a matrix suitable for processing using CNNs. Fig. 4(a)–(d) displays the gamma–ray curves, actual and seismic lithology labels, and borehole-side seismic data, respectively. By using the logging interpretation, lithological logs can be accurately classified into gas sandstone, non-gas sandstone, and mudstone, as shown in Fig. 4(b). These classifications are subsequently converted into seismic lithology labels through down-sampling, as illustrated in Fig. 4(c). By using a 'point-window' matching sampling strategy (as shown in Fig. 5), geological information specific to certain points and time depths was combined with neighboring seismic data samples. This approach effectively links logging data with seismic waveforms. Following this, the seismic data within the time window that matched the logging data were transformed into the T-F spectrum using the proposed ISD method, as illustrated in Fig. 4(f). The use of overlapping sliding time windows enables the creation of 2-D T-F spectral maps and the corresponding seismic lithology labels, which were used as inputs for the CNN, as shown in Fig. 4(f). To speed up the training of our proposed DL models, we set the frequency range of each T-F map to 10–80 Hz with a frequency sampling interval of 1 Hz.

To obtain accurate lithology labels, we extracted source wavelets using available well and seismic section data above 50 ms using Hampson_Russell software. The extracted wavelets are presented in Fig. 6(a). The extracted wavelet amplitude–frequency spectrum was obtained using a Fourier transform, as shown in Fig. 6(b). Fig. 6(b) shows that the dominant frequency of the wavelets was approximately 30 Hz. The target area velocity was approximately 3500 m/s from well-logging. The traditional seismic vertical resolution is $\lambda/4$, which corresponds to 29 m. Moreover, Fig. 6(c) shows the depth difference in the sample rate, which is obtained from the depth-time conversion curve. From Fig. 6(c), it is clear that at a sampling rate of 4 ms, the thinnest sandstone identifiable is approximately 5 m. Although the original logging data were sampled at 0.125 m intervals, significantly exceeding the seismic data resolution, these thin layers may not exhibit distinct T-F features in the seismic data owing to the limited resolution. If the lithology within a 4 ms interval in the lithology log is labeled in the lithology log based on predominant lithology type (occupying more than one-third of the interval), this method generally provides reliable results. However, when the lithology types within the 4 ms interval are more evenly distributed, assigning the interval to a single lithology type becomes less appropriate and may introduce inaccuracies. To address this limitation, we refined the borehole-side seismic lithological labels by representing them as probability distributions. This probabilistic approach eliminated the rigidity of traditional hard-label definitions and provided a more nuanced representation of the lithology (as shown in Fig. 7). The processed seismic lithology labels for wells 1 and 2 are shown in Fig. 8.

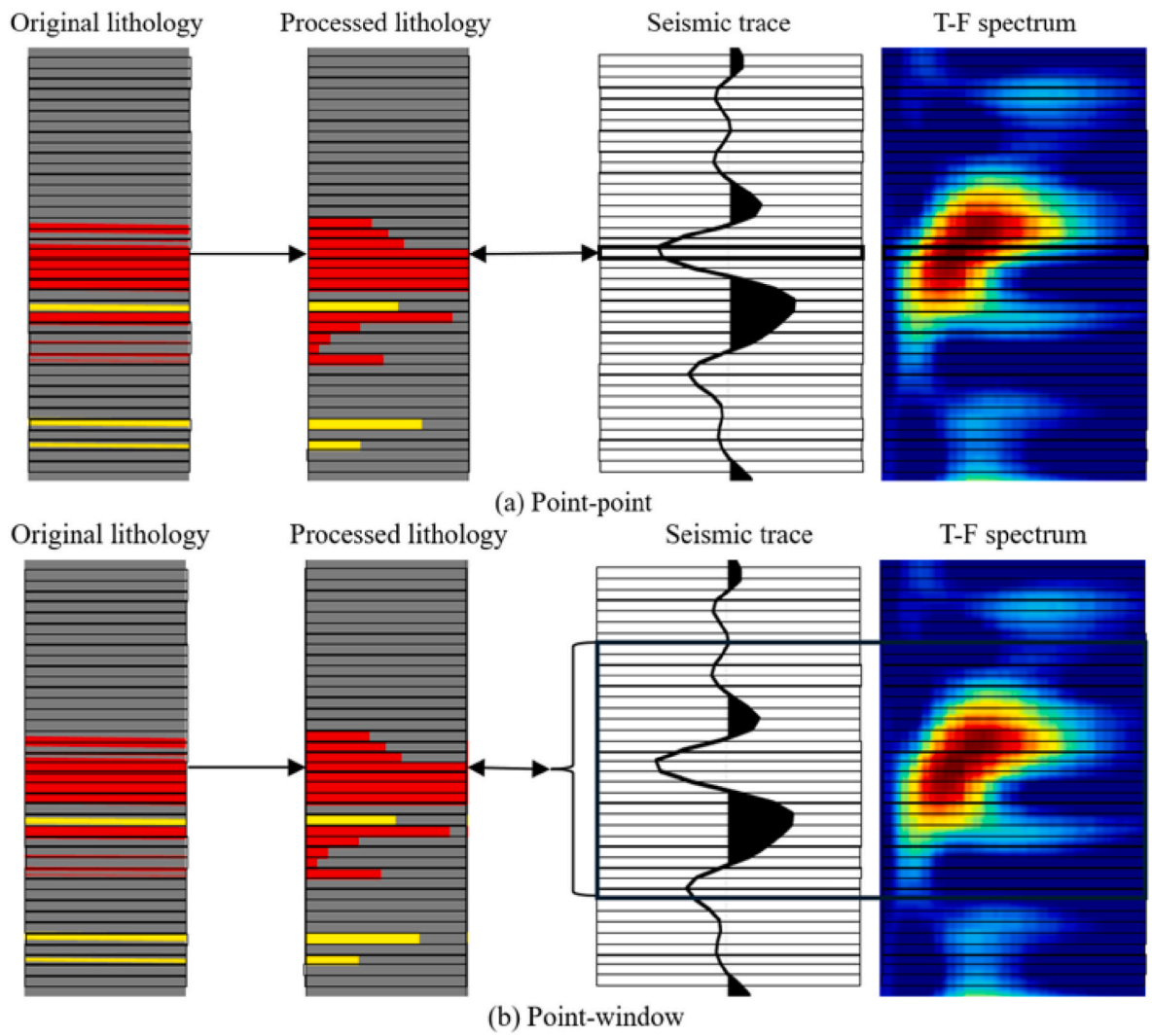

Fig. 5. The sampling 'point-window' matching strategy.

2.4. The overall architecture

An overview of the seismic reservoir prediction system based on the proposed method is presented in Fig. 9. Initially, seismic data from the study area underwent preprocessing, resulting in 2-D T-F spectral maps generated using the proposed ISD method. Before training the CNN, all 2-D T-F spectral maps were divided into training, validation, testing, and prediction sets. The T-F spectral maps from borehole-side seismic data were evenly partitioned into training, validation, and testing sets, while the T-F spectral maps from other traces were designated as the prediction set to predict the entire profile. After training, the trained AdaBoost-CNN method was evaluated using the testing set, and the prediction results were quantified using the prediction set in combination with the proposed AdaBoost-CNN method.

3. Field case application

The study area is located in the mouth of the Pearl River Basin in the South China Sea. The reservoir formation is sandstone, and the upper and lower layers around the reservoir are composed of mudstone. Fig. 10 shows the cross-well profiles of the post-stack seismic data. It contains 300 seismic traces, each with 119 sampling points. The sampling interval was 4 ms. The target zone was set at 2890–3715 m in depth, and the corresponding time range was 3200–3676 ms. The black curved lines in Fig. 10 illustrate gamma-ray logging.

3.1. Field data tests for the proposed ISD

The accuracy of ISD in the T-F analysis was evaluated using field seismic data. In Fig. 11, the T-F spectra of the seismic data from wells 1 and 2 are presented. Fig. 11(a) displays the seismic data of well 1, whereas Fig. 11(b) and (c) illustrate the T-F spectra using the CWT and proposed ISD method, respectively. Fig. 11(d) shows the seismic data of well 2, with Fig. 11(e) and (f) illustrating its T-F results using the CWT and proposed ISD method, respectively.

The proposed ISD method exhibits higher time and frequency resolutions in the T-F spectra, as highlighted by the red circle in Fig. 11. Additionally, it is evident that this method effectively suppresses 'artifacts', as indicated by the red arrows. This effectiveness is attributed to the superior performance of the non-convex L_{1-2} regularization method in achieving optimal solutions. Therefore, in this study, the T-F spectral maps generated by the proposed ISD method were used as input samples for DL, which enabled their frequency features to be accurately learned.

3.2. Proposed approach performance evaluation

A series of comparative experiments were conducted to evaluate the effectiveness of the proposed method. This evaluation used the three borehole-side seismic traces from two wells (six traces in total). Traces 63, 64, and 65 are the borehole-side seismic traces of well 1, and traces 240, 241, and 242 are the borehole-side seismic traces of well 2. The

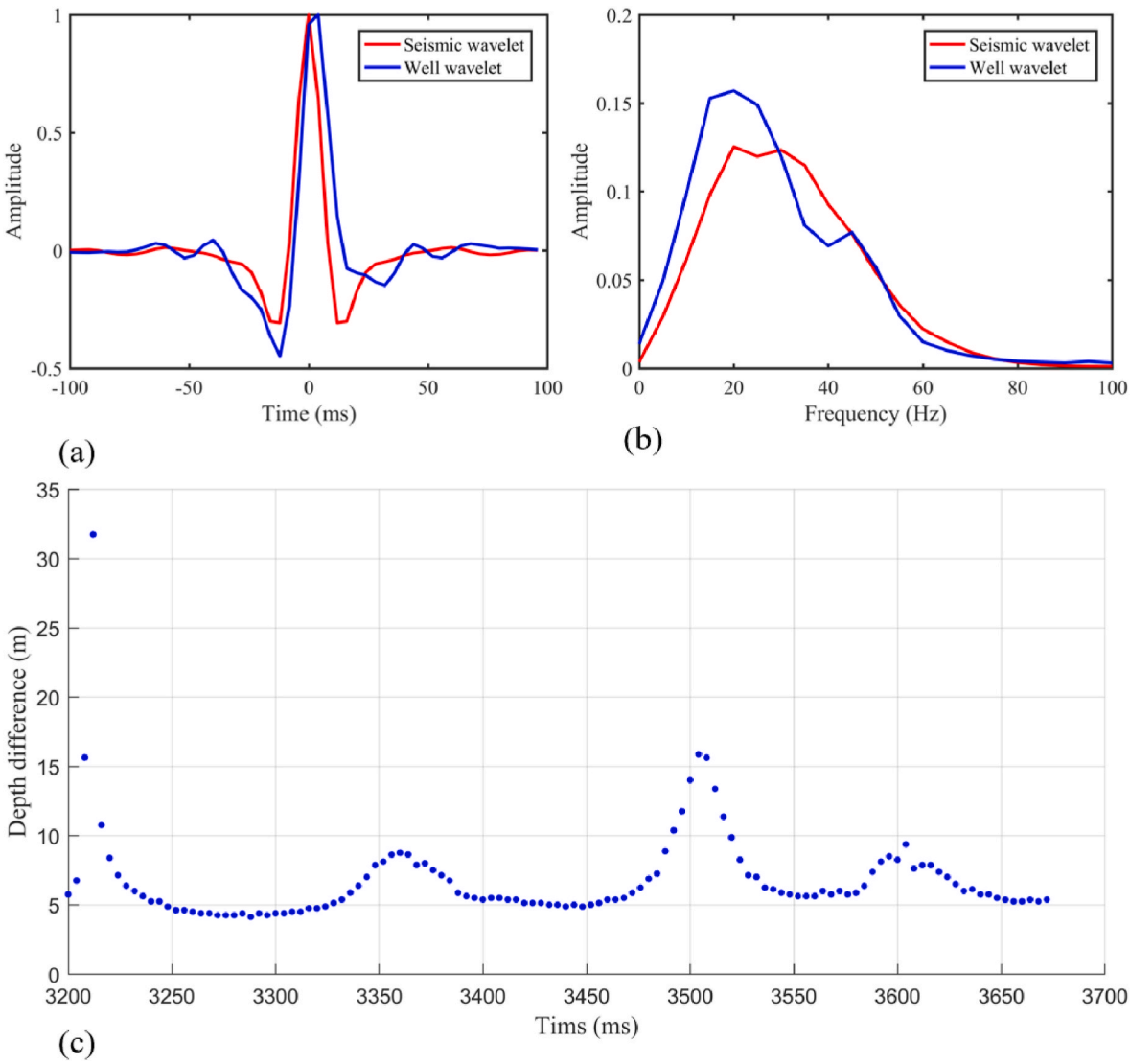

Fig. 6. (a) source wavelet; (b) source wavelet amplitude–frequency spectrum; (c) depth difference in the sample rate.

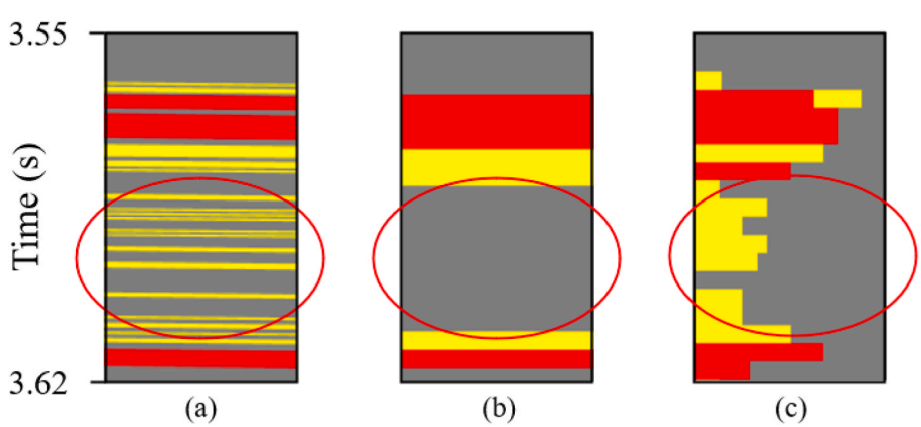

Fig. 7. (a)–(c) represent the lithology distribution between 3.55 and 3.62 s for well 2; (a) actual lithology labels. (b) seismic lithology determined based on the dominant lithological type; and (c) probability distribution of the lithology determined by the statistical proportions of the lithology types.

seismic lithology labels from the same borehole-side were treated as identical. The borehole-side seismic traces were divided into training, validation, and testing sets. Traces 64 and 241 were used as the training set, traces 65 and 242 as the validation set, and traces 63 and 240 as the testing set. To optimize model parameters and evaluate performance during training, the training set was further split into multiple folds using cross-validation. In this process, one-fold was used as the validation fold for parameter selection, while the remaining folds were used

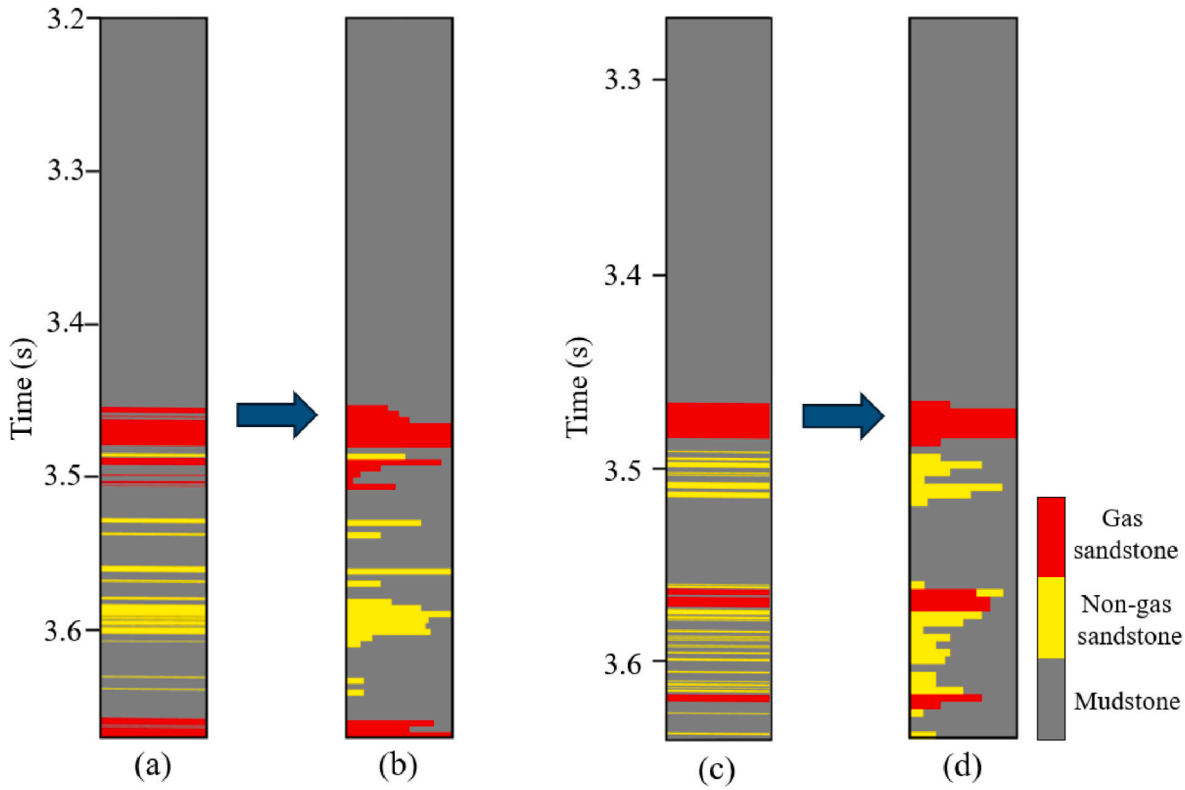

Fig. 8. (a) and (c) actual lithological distributions of wells 1 and 2; (b) and (d) preprocessed seismic lithology labels.

for training. The validation set used during training to monitor overfitting. The test set remained independent throughout and was used solely to assess the generalization performance of the final model.

As previously mentioned, the seismic lithology can be predicted using the CWT-CNN method (Zhang et al., 2018). By combining the proposed ISD method and a CNN, an ISD-CNN was also developed in this study. To evaluate the performance of AdaBoost-CNN, the CWT and proposed ISD method were combined with AdaBoost-CNN (CWT-AdaBoost-CNN and ISD-AdaBoost-CNN, respectively). Comparative tests were performed using an Intel (R) Core (TM) i3-12300 @ 3.50 GHz processor, equipped with a 16.0 GB installed memory (RAM) on a 64-bit Windows 11 operating system, using the built-in Python library to measure the time for both the AdaBoost-CNN and traditional AdaBoost methods without CNN transfer. The CNN was compiled using the categorical cross-entropy loss function, Adam optimizer, and cross-entropy as metrics. The Adam learning rate was fixed at 0.001. Additionally, if the cross-entropy error in the validation did not decrease for four consecutive epochs, an early stopping mechanism was triggered. The initial CNN configuration sets the number of epochs to 10 and the batch size to 32.

To thoroughly evaluate the performance of the proposed approach, the root-mean-squared error (RMSE) and coefficient of determination (R^2) were calculated using Eqs. (10) and (11), as the evaluation metrics.

The RMSE is a measure of the standard deviation of the differences between predicted and true values. This value was calculated using the following formula:

$$RMSE = \sqrt{\frac{1}{N}\sum_{i=1}^{N}(y_i - \hat{y}_i)^2} \tag{10}$$

R^2 is a metric that measures the goodness of fit of a model to the data and reflects its ability to explain the variability of the target variable. This was calculated as follows:

$$R^2 = 1 - \frac{\sum_{i=1}^{N}(y_i - \hat{y}_i)^2}{\sum_{i=1}^{N}(y_i - \bar{y})^2} \tag{11}$$

where N is the total number of samples, y_i is the true value of the ith sample, $\hat{y}_i$ is the predicted value of the ith sample, and $\bar{y}$ is the mean of all true values. A smaller RMSE indicates better predictive performance, ideally approaching 0. For R^2, a value closer to one indicates a better model fit to the data.

3.2.1. Sample length effects

To fully evaluate the impact of the input sample length on model performance, we conducted five-fold cross-validation on the training sets using CWT-CNN, ISD-CNN, CWT-AdaBoost-CNN, and ISD-AdaBoost-CNN. The CVM-RMSE (RMSE cross-validation-mean) and CVM-R^2 (R^2 cross-validation-mean) results are shown in Fig. 12(a)–(d).

From Fig. 12(a) and (b), it can be observed that the CVM-RMSE of AdaBoost-CNN-based methods was consistently lower than that of traditional CNNs across all sample lengths, on both the training and testing sets. This indicates that the proposed method can better minimize errors better through the dynamic adjustment of sample weights, allowing the model to effectively focus on samples that are more challenging to predict. Additionally, the results demonstrated that the CVM-RMSE decreased as the sample length increased, suggesting that longer sample lengths enabled the models to capture more comprehensive seismic data.

In Fig. 12(c) and (d), the CVM-R^2 of the AdaBoost-CNN-based methods was significantly higher than that of traditional CNNs, particularly for ISD-AdaBoost-CNN. This highlights the effectiveness of the proposed method in improving the ability of the model to explain the variability in seismic data. Notably, for both CVM-RMSE and CVM-R^2, the ISD-based methods outperformed the CWT-based methods, particularly when combined with AdaBoost-CNN. This confirms that the

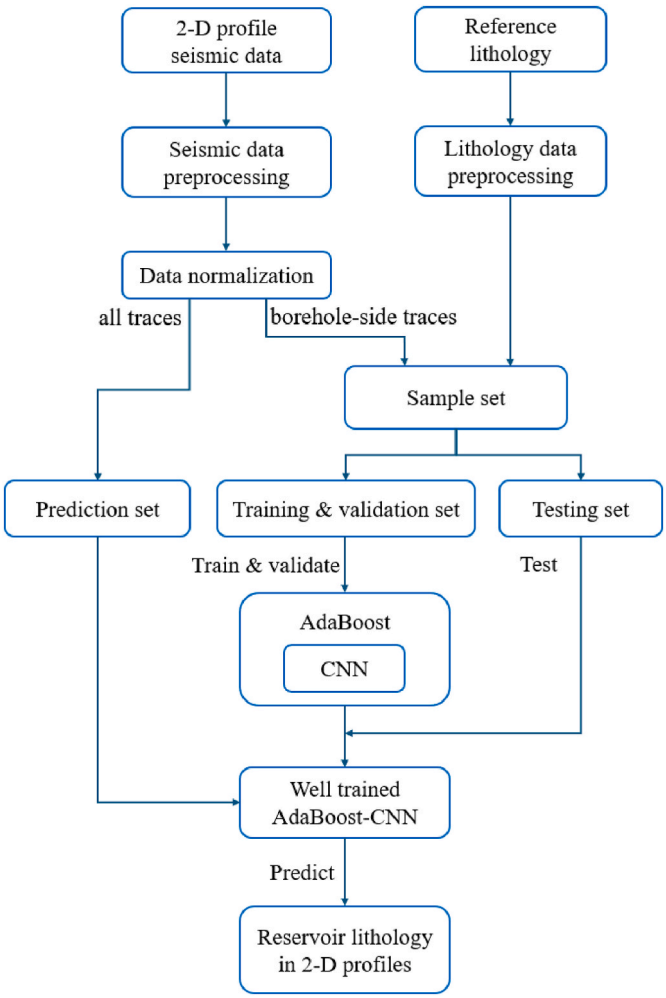

Fig. 9. Workflow diagram for the proposed method.

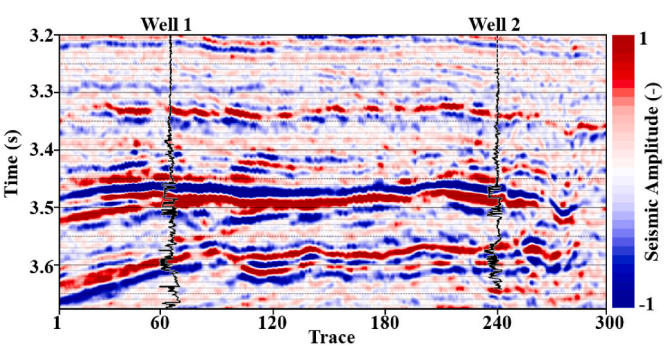

Fig. 10. Seismic profile through wells 1 and 2.

higher resolution of the ISD T-F spectral maps provided additional informative features, enabling the model to achieve better performance.

It is also worth noting that whereas the performance generally improved with increasing sample length, the results indicated that a sample length of 25 yielded a balance between training and testing performances. For example, at this sample length, the CVM-R^2 of testing data achieved one of its highest values. As the seismic sample time interval was 4 ms, this corresponded to a time window of 100 ms, which was found to be optimal for fully capturing and utilizing the frequency information in our seismic data and model.

In summary, the experimental results demonstrate that the proposed AdaBoost-CNN framework, particularly when using ISD T-F spectral maps as input, efficiently captures the essential characteristics of seismic data, improves the generalization performance, and leverages the advantages of higher-resolution T-F spectral maps over traditional CWT inputs.

3.2.2. Computation time analysis

Table 1 compares the performance of the traditional AdaBoost-CNN (without CNN transfer) and the proposed AdaBoost-CNN (with CNN transfer) on the ISD-based training, validation, and testing sets. The training set was used for model training, the validation set for preventing overfitting, and the test set for evaluating the final model's performance. These T-F maps are used as input samples to demonstrate the effectiveness of the proposed method (with a fixed number of estimators = 10). The Proposed AdaBoost-CNN achieved training and testing RMSE of 0.1 and 0.107, respectively, and training and testing R^2 of 0.824 and 0.796, respectively, after 10 epochs, with a computation time of only 94.84 s. As the number of training epochs increased to 30 and 40, the Proposed AdaBoost-CNN reached optimal training and testing RMSE values of 0.078 and 0.085, respectively, while the training and testing R^2 stabilized at 0.893 and 0.87, respectively, with computation time maintained at approximately 103 s. Compared to the traditional AdaBoost-CNN over the same epochs, the Proposed AdaBoost-CNN significantly reduced redundant computations during training through the CNN transfer strategy. It also improved both the model's fitting ability on the training data (lower Training RMSE and higher Training R^2) and its predictive performance on the testing data (lower Testing RMSE and higher Testing R^2).

The impact of the number of estimators on the performance of the Proposed AdaBoost-CNN (with a fixed epoch count of 30) is detailed in Table 2. It is evident that as the number of estimators increases, the training and testing performance of the Proposed AdaBoost-CNN steadily improves, indicating that the model's fitting ability on the training data continues to enhance, with better performance on the testing set. However, when the number of estimators exceeds 20, the improvement in testing performance gradually diminishes, showing diminishing marginal returns. At the same time, the computation time increases significantly, highlighting the need to balance model complexity and computational cost in practical applications. When the number of estimators exceeds 30, the improvement in test performance is no longer evident. Therefore, we chose 30 epochs and 30 estimators as the parameter selection for the model.

3.2.3. Overall performance test

The performance of the proposed method was evaluated on the testing sets. Figs. 13 and 14 illustrate the prediction results for traces 63 (Fig. 13(a)) and 240 (Fig. 14(a)), respectively. Fig. 13(b) and 14(b) show the seismic lithology labels of wells 1 and 2, respectively. Fig. 13(c)–(e), (g), and (i), and 14(c), (e), (g), and (i) illustrate the lithology probability distribution prediction results of the CWT-CNN, ISD-CNN, CWT-AdaBoost-CNN, and ISD-AdaBoost-CNN, respectively. Fig. 13(d)–(f), (h), and (j) and 14(d), (f), (h), and (j) show the probability for each class, with color proportions indicating probability.

In Fig. 13, compared to the CWT-CNN (Fig. 13(c) and (d)), the ISD-CNN (Fig. 13(e) and (f)) provides predictions that are closer to the seismic lithology with higher confidence levels in the probability maps. This indicates that the ISD method can generate high-resolution T-F spectral maps, enabling DL models to better capture feature information in the frequency domain and produce more accurate probability prediction results. By integrating AdaBoost, the recognition ability for complex reservoirs was significantly improved. ISD-AdaBoost-CNN (Fig. 13(i) and (j)) achieved the most accurate predictions for gas sandstone and thin reservoirs (as highlighted by the red dashed box and black arrows), with a noticeably higher prediction confidence for gas sandstone in the probability maps compared to those of the other models. As shown in Fig. 14, ISD-AdaBoost-CNN can accurately identify

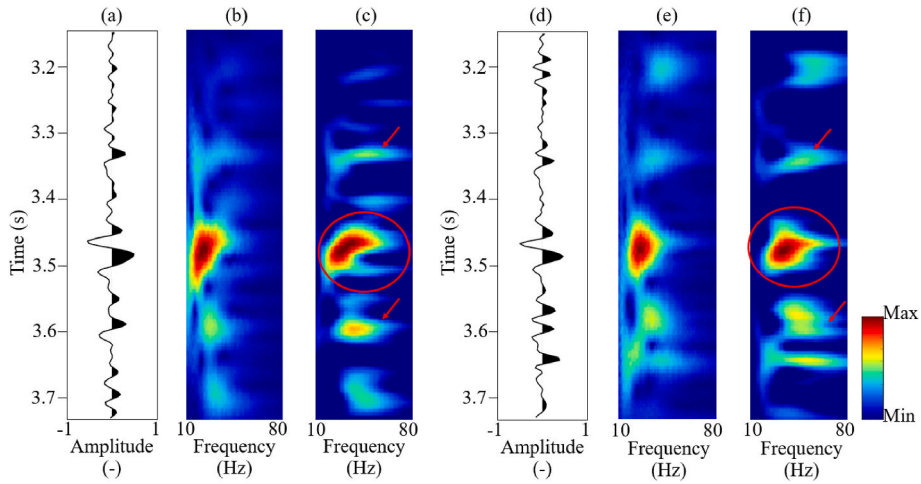

Fig. 11. T-F spectral results of the CWT and proposed ISD method; (a)–(c) seismic data at well 1 and its T-F spectra obtained by the CWT and proposed ISD method; (d)–(f) seismic data at well 2 and its T-F spectra obtained by the CWT and proposed ISD method.

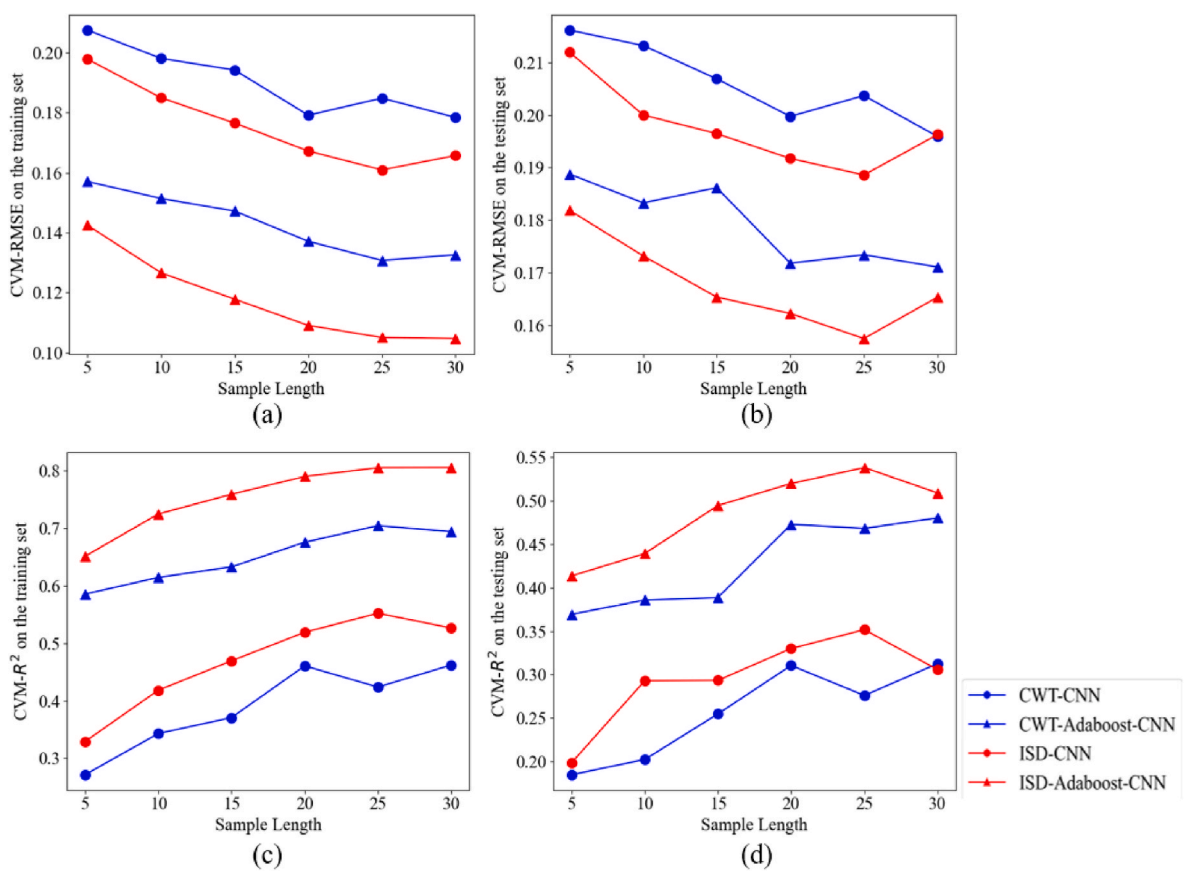

Fig. 12. Input sample length effects on the training sets for CWT-CNN, ISD-CNN, CWT-AdaBoost-CNN and ISD-AdaBoost-CNN.

thin reservoirs, particularly in complex lithological regions (highlighted by the red dashed box and black arrows). Its probability maps were closer to the actual lithology labels, demonstrating its remarkable advantage for high-resolution predictions.

Table 3 presents the quantitative evaluation results of regression performance. The results show that both the CWT-CNN and ISD-CNN underperformed compared with their AdaBoost-enhanced counterparts. The CWT-CNN achieved an RMSE of 0.148 and R^2 of 0.629, indicating limited prediction accuracy and model fit. Although the ISD-CNN improved the performance with an RMSE of 0.111 and an R^2 of 0.780, it still fell short in capturing the full complexity of the reservoir characteristics.

In contrast, ISD-AdaBoost-CNN significantly outperformed all other models, achieving the lowest RMSE of 0.076 and the highest R^2 of 0.897. This demonstrates its superior ability to predict reservoir properties with high precision and accuracy. The combination of high-resolution ISD T-F spectra and the ensemble learning power of AdaBoost enabled the model to better capture critical features and achieve exceptional regression performance.

Additionally, a comparison between ISD-AdaBoost-CNN and CWT-

Table 1
Performance of different models on the training and testing set (estimators = 10).

Method	Epochs	Training RMSE	Testing RMSE	Training R^2	Testing R^2	Computation Time (Sec.)
AdaBoost-CNN without CNN transfer	10	0.149	0.153	0.615	0.597	106.12
	20	0.112	0.114	0.78	0.77	182.03
	30	0.101	0.106	0.82	0.803	258.14
	40	0.096	0.1	0.838	0.824	302.88
Proposed AdaBoost-CNN	10	0.1	0.107	0.824	0.796	94.84
	20	0.082	0.091	0.882	0.852	101.17
	30	0.078	0.085	0.893	**0.87**	103.05
	40	0.078	0.085	0.893	0.87	103.15

Table 2
Performance of different models on the training and testing set (epochs = 30).

Method	Estimators	Training RMSE	Testing RMSE	Training R^2	Testing R^2	Computation Time (Sec.)
Proposed AdaBoost-CNN	10	0.078	0.085	0.893	0.87	100.75
	20	0.068	0.082	0.921	0.88	194.12
	30	0.06	0.076	0.938	**0.897**	280.05
	40	0.056	0.073	0.946	0.906	365.67
	50	0.053	0.07	0.952	0.912	478.76
	100	0.045	0.063	0.965	0.929	995.19

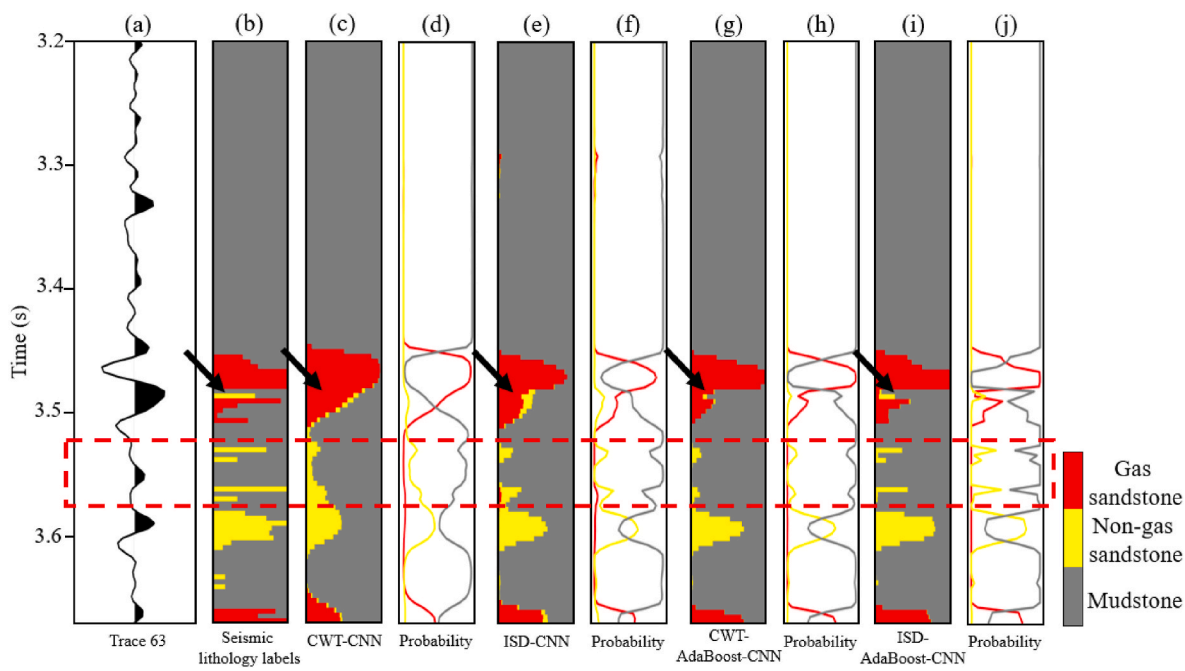

Fig. 13. Trace 63 prediction results; (a) trace 63 seismic data; (b) seismic lithology probability distribution; and (c)–(j) reservoir probability distribution prediction results and their corresponding probabilities using CWT-CNN, ISD-CNN, CWT-AdaBoost-CNN, and ISD-AdaBoost-CNN.

AdaBoost-CNN (R^2: 0.897 versus 0.783) highlights the advantages of ISD in providing richer feature information, further enhancing the predictive capability of DL models in complex seismic reservoir analyses.

Fig. 15 illustrates the relationship between the predicted and true probabilities for three categories: gas and non-gas sandstone, and mudstone. The solid black line represents the ideal prediction line, in which the predicted probability perfectly matches the true probability. The dashed lines serve as reference lines, indicating the tolerance range. Points within the dashed lines indicate that the prediction error is small, reflecting higher model reliability, whereas points outside the dashed lines indicate larger deviations and less accurate predictions.

It is evident from Fig. 15 that the predictive performance varied across the models. Among them, the ISD-AdaBoost–CNN (Fig. 15(d)) demonstrated the highest prediction accuracy because most data points fell within the tolerance range, indicating smaller prediction errors across categories. In contrast, other models, such as CWT-CNN and ISD-CNN, showed relatively large prediction deviations, particularly in the gas and non-gas sandstone categories.

In summary, ISD-AdaBoost-CNN significantly improved classification accuracy, demonstrating strong classification capability and robustness. This indicates that AdaBoost and CNN transfer have significant advantages for improving CNN classification performance, particularly in addressing the class imbalance problem.

3.3. Analysis of seismic reservoir quantitative prediction results

The 2-D seismic data shown in Fig. 8 were used to test the proposed method. Fig. 16(a) and (c) show the probability prediction results of the CWT-CNN for the 2-D profiles of gas and non-gas sandstone. Fig. 16(b) and (d) show the probability prediction results of ISD-CNN for the same

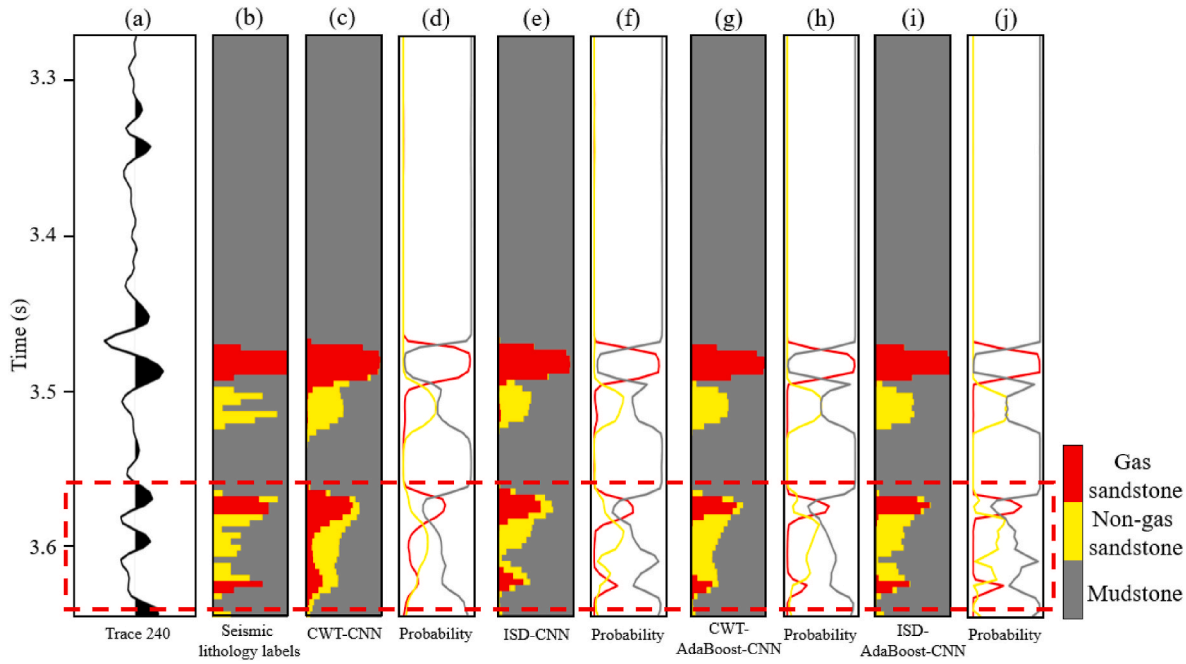

Fig. 14. Trace 240 prediction results; (a) trace 63 seismic data; (b) seismic lithology probability distribution; and (c)–(j) reservoir probability distribution prediction results and their corresponding probabilities using CWT-CNN, ISD-CNN, CWT-AdaBoost-CNN, and ISD-AdaBoost-CNN.

Table 3
Performance of different models on the test set.

Method	RMSE	R^2
CWT-CNN	0.148	0.629
ISD-CNN	0.111	0.78
CWT-AdaBoost-CNN	0.111	0.783
ISD-AdaBoost-CNN	**0.076**	**0.897**

lithologies. Both CWT-CNN and ISD-CNN can identify certain gas sandstones. The prediction results of the CWT-CNN more accurately indicated the locations of the gas sandstone while demonstrating good lateral continuity. When identifying non-gas sandstone, the ISD-CNN can reveal thin layers (red marker circles) that the CWT-CNN cannot recognize even though these layers are sparsely distributed in the lithology.

Fig. 17(a) and (c) show the probability prediction results of CWT-AdaBoost-CNN for the 2-D profiles of gas and non-gas sandstone. Fig. 17(b) and (d) show the probability prediction results of ISD-AdaBoost-CNN for the same lithologies. Compared with Fig. 16, both the CWT-AdaBoost-CNN and ISD-AdaBoost-CNN exhibited greater stability and more precise contours than the CWT-CNN and ISD-CNN. This indicates that the AdaBoost-CNN method significantly improved the CNN prediction precision. Comparing Fig. 17(c) with Fig. 17(d), the ISD-AdaBoost-CNN demonstrated better recognition capability for thin non-gas sandstone layers interbedded within mudstone and more accurately depicted the non-gas sandstone contours, as indicated by the red circles. These results suggest that ISD-AdaBoost-CNN provides higher recognition accuracy and presents a more realistic geological representation.

We used the category with the highest probability prediction results from these models as the final 2-D reservoir lithology prediction result, as shown in Fig. 18. Among these methods, the ISD-AdaBoost-CNN model (d) produced the most accurate and continuous lithology predictions, particularly for thin gas sandstones and thin non-gas sandstones, as highlighted by the red arrows. This demonstrated that the combination of ISD and AdaBoost techniques effectively improves the prediction accuracy of thin layers while maintaining good continuity. After integrating AdaBoost in the CWT-AdaBoost-CNN model (c), the ability to capture underrepresented lithology classes, such as thin gas sandstone layers, was significantly enhanced, as indicated by clearer red and yellow regions. However, the ISD-AdaBoost-CNN model (d) further refined these results, highlighting the importance of ISD in generating high-resolution T-F spectral features. This underscores the superiority of the ISD-AdaBoost-CNN model in addressing challenges associated with identifying thin sandstone layers.

4. Discussion

For all models, thick sands are easier to predict due to their clear reflective characteristics. All thick sands, especially thick gas sandstones, near Wells 1 and 2 can be predicted using various models, even with training data from only one well (the black dashed regions in Figs. 19 and 20)). These results shown that the DL-based lithology prediction methods have great potential in the field of seismic exploration. Compared with other models, the medium and the thin sandstones, mixed with mudstone and unevenly distributed, can be predicted by our proposed method (the red dashed regions in Figs. 19 and 20). However, it is evident from Figs. 19 and 20 that the accuracy of lithology prediction results has significantly decreased compared to Figs. 13 and 14. When training with data from a single well, the amount of data may be relatively limited. This can prevent the model from fully learning the complex mapping relationship between lithology and seismic data, thereby affecting prediction accuracy. In our study, we used borehole-side seismic traces and lithology classifications from well-logging as training and testing sets. We assumed that reservoir lithology exhibits lateral continuity within a certain distance, allowing lithology labels to be approximated based on spatial proximity (Fig. 21). Although the effectiveness of this strategy was confirmed by the experimental results, the scarcity of well-logging remains a challenging issue for the application of deep learning in seismic exploration (Goyes-Peñafiel et al., 2024; Jo et al., 2024; Jordão et al., 2022).

The training set accounted for approximately 66% of the whole data, including sufficient samples of mudstone and medium-to-thick sands. However, thin sands were underrepresented and influenced by adjacent lithologies, making it difficult for traditional models to learn the T-F characteristics. To address class imbalance, our method used AdaBoost's

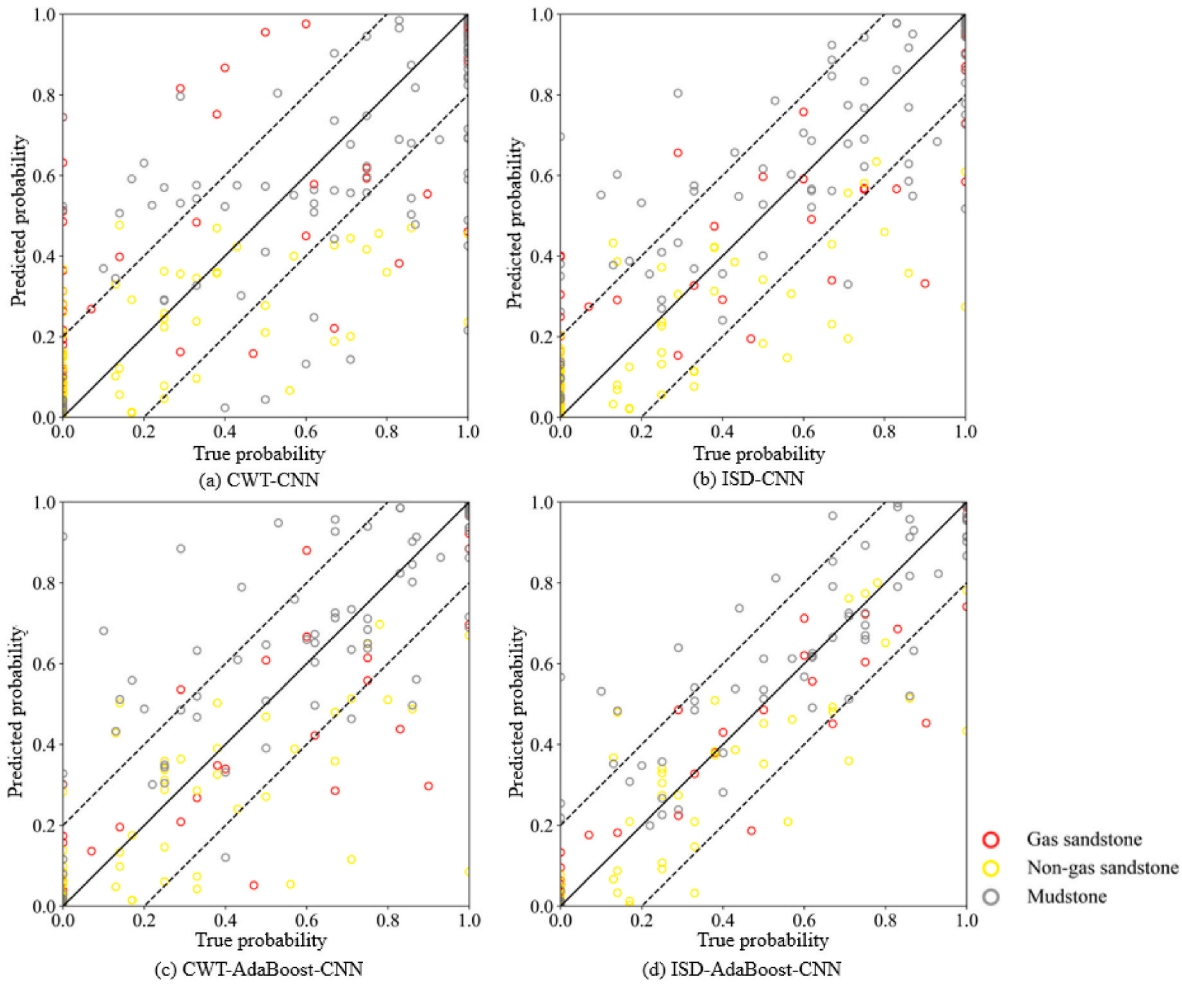

Fig. 15. Predicted and true probability scatter plots for different models and categories on the test set. The figure illustrates the relationship between predicted and true probabilities for three categories: "gas sandstone," "non-gas sandstone," and "mudstone."

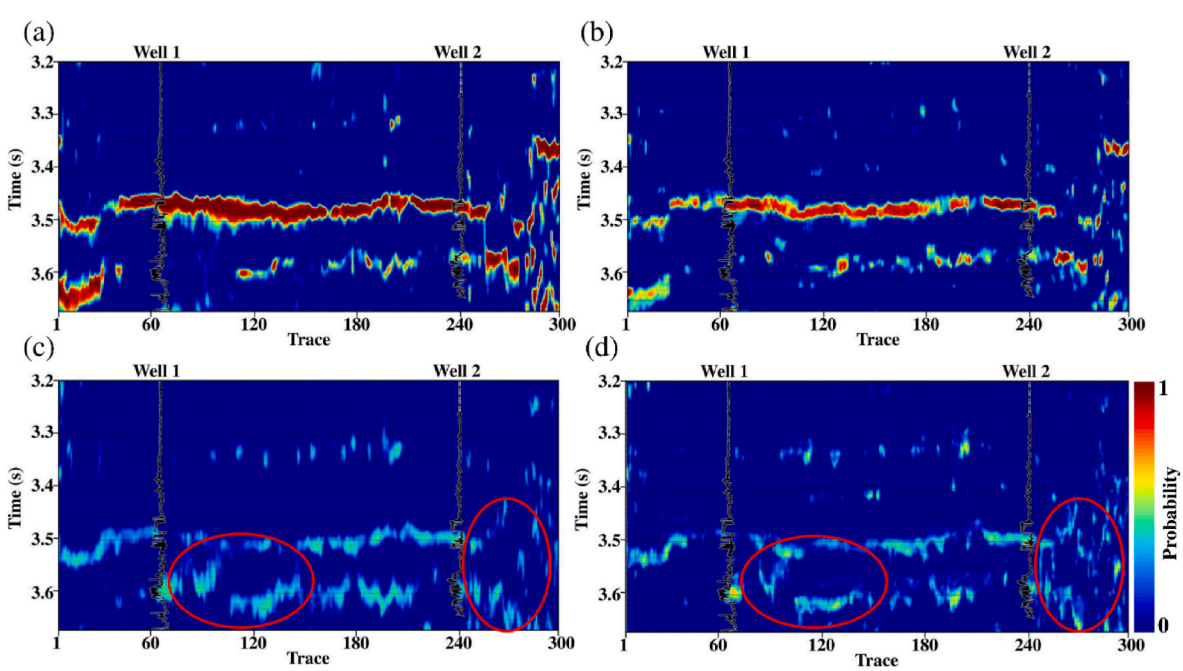

Fig. 16. 2-D profile of reservoir prediction probability; (a) and (b) probability distribution of gas sandstone in CWT-CNN and ISD-CNN, respectively; (c) and (d) probability distribution of non-gas sandstone in CWT-CNN and ISD-CNN, respectively. The black curved lines illustrate gamma-ray logging.

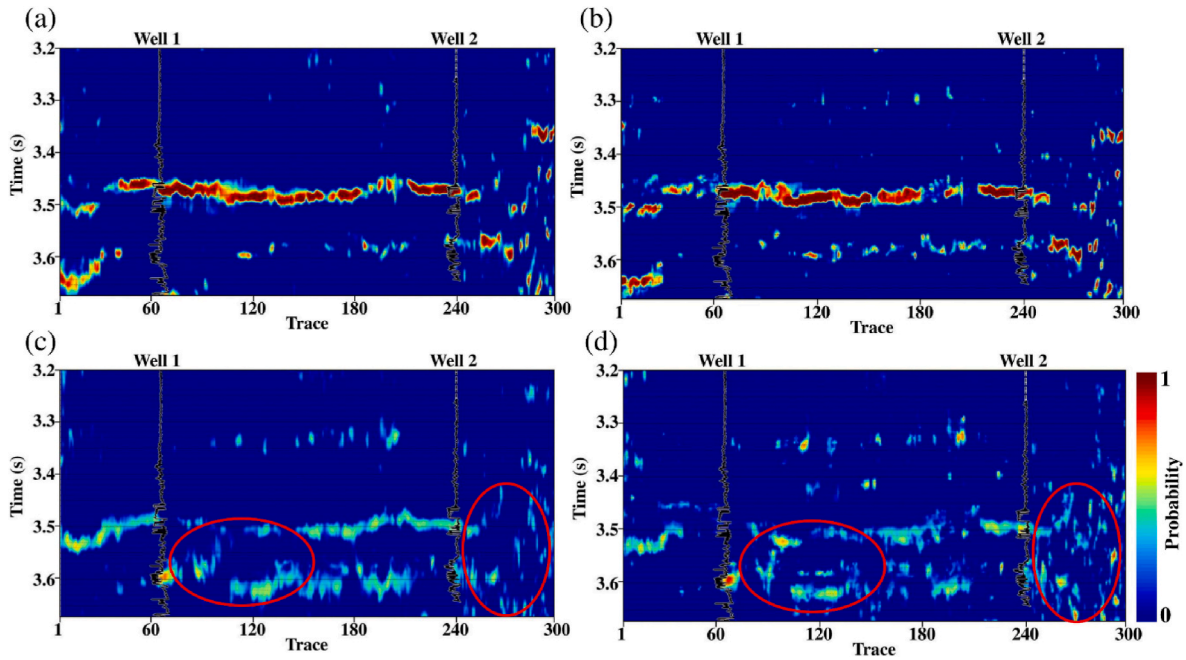

Fig. 17. 2-D profile of reservoir prediction probability; (a) and (b) probability distribution of gas sandstone in CWT-AdaBoost-CNN and ISD-AdaBoost-CNN, respectively; (c) and (d) probability distribution of non-gas sandstone in CWT-AdaBoost-CNN and ISD-AdaBoost-CNN, respectively. The black curved lines illustrate gamma-ray logging.

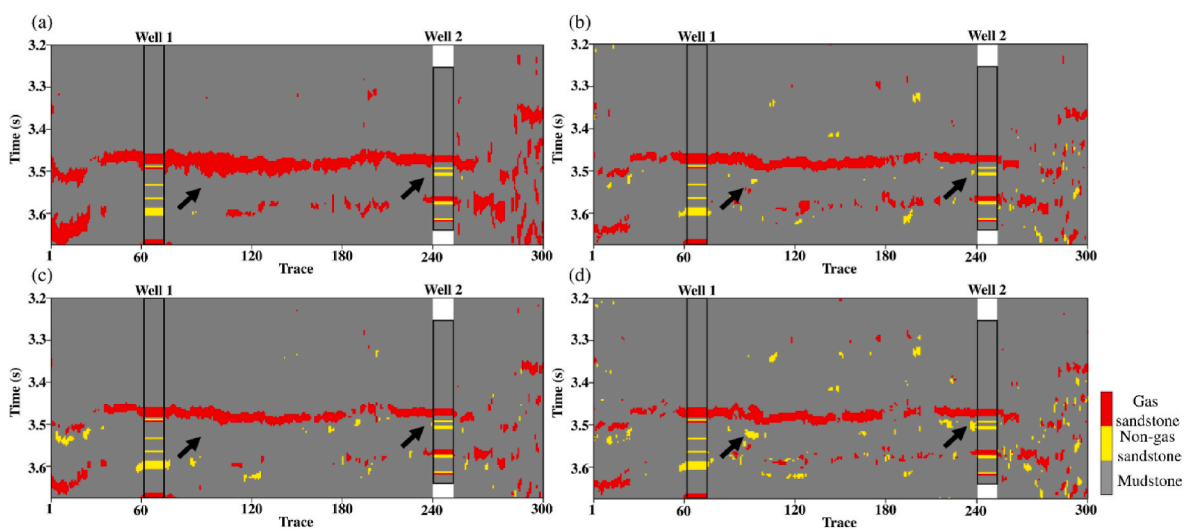

Fig. 18. 2-D profiles of the prediction reservoir lithology by CWT-CNN (a), ISD-CNN (b), CWT-AdaBoost-CNN (c) and ISD-AdaBoost-CNN (d), respectively.

sample weight adjustment strategy. This increased the focus on under-represented classes, such as thin sands, resulting in higher prediction accuracy of these samples. However, this approach sacrificed some lateral continuity, especially in geologically complex regions (Fig. 19), which is difficult to avoid under such conditions.

In this study, the proposed AdaBoost method reduced training time compared to the original AdaBoost while maintaining similar prediction performance. This is attributed to a "CNN transfer" mechanism, which allows weight inheritance among base estimators within the AdaBoost framework. Early stopping was applied to terminate training once validation loss stopped improving, preventing overfitting and redundant computations. However, achieving better results still requires additional time. We conducted multiple experiments to determine the best parameters for our task, such as the T-F window size (sample length), the number of CNN epochs, and the number of AdaBoost iterations (number of estimators). The architecture design and parameter selection of the ISD-AdaBoost-CNN model heavily relied on time-consuming experiments or experience. Both the accuracy and efficiency are important for a method to be widely applied. How to make models automatically and efficiently select optimal parameters is one of the key problems for future research. Integrating deep learning with optimization techniques, such as particle swarm optimization and genetic algorithm, may help address this challenge (Czako et al., 2021; Haixiang et al., 2016; Zhang et al., 2022).

5. Conclusion

This study proposes a novel DL approach for seismic lithology prediction by combining ISD and AdaBoost-CNN. The proposed ISD method produces higher-resolution and more focused T-F spectral maps. These

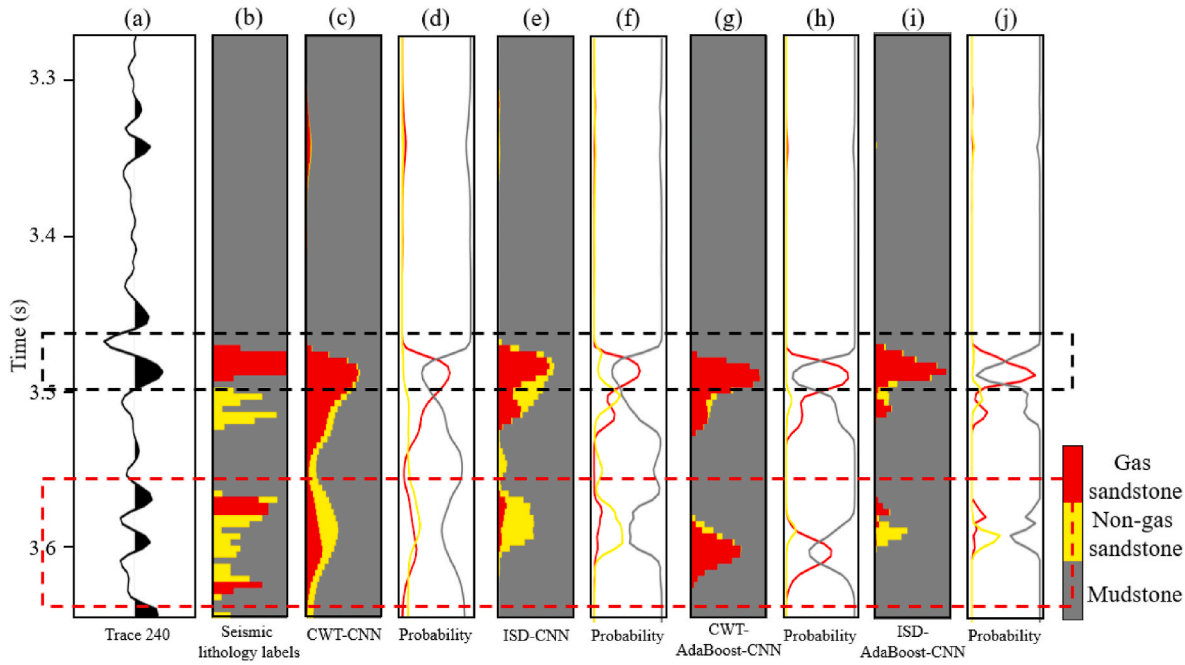

Fig. 19. The prediction results of trace 240 (trace 64 as training, 65 as validation). (a) seismic data of trace 240. (b) seismic lithology labels. (c)–(j) probability distribution prediction results of reservoirs and its corresponding probability using CWT-CNN, ISD-CNN, CWT-AdaBoost-CNN, and ISD-AdaBoost-CNN.

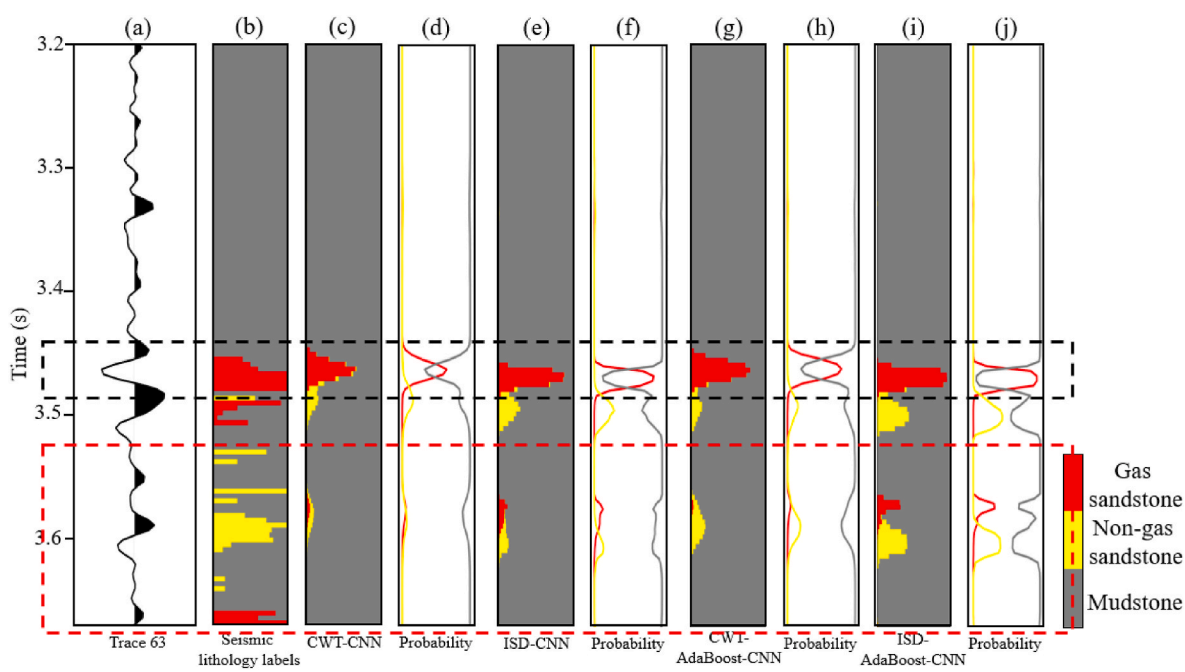

Fig. 20. The prediction results of Trace 63 (trace 241 as training, 242 as validation). (a) seismic data of trace 63. (b) seismic lithology labels. (c)–(j) probability distribution prediction results of reservoirs and its corresponding probability using CWT-CNN, ISD-CNN, CWT-AdaBoost-CNN, and ISD-AdaBoost-CNN.

maps were used as inputs for DL, which enabled the effective extraction of frequency information from seismic data. The AdaBoost-CNN can effectively solve the problems of an unbalanced class, which is suitable for seismic lithology prediction. This study evaluated the performance of the proposed AdaBoost-CNN for post-stack seismic lithology prediction under various influencing factors. The test results showed that AdaBoost-CNN had a higher generalization ability. Additionally, comparative experiments were conducted using 2-D field seismic data. The proposed method provided quantitative probability prediction results. These results demonstrated that the proposed approach improved the accuracy of seismic lithology predictions, indicating its potential for future applications in this field.

CRediT authorship contribution statement

Wenliang Nie: Writing – original draft, Methodology. **Jiayi Gu:** Writing – original draft, Software, Data curation. **Bo Li:** Writing – review & editing. **Xiaotao Wen:** Writing – review & editing. **Xiangfei Nie:** Writing – review & editing, Supervision.

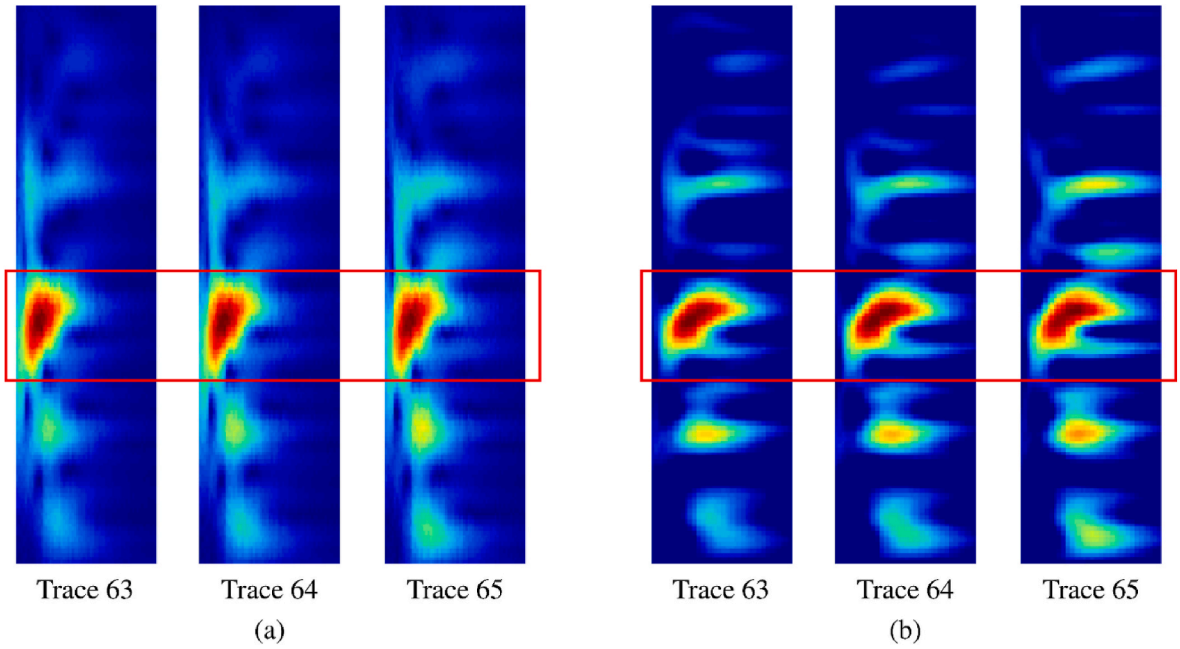

Fig. 21. T-F spectra of traces 63, 64, and 65, obtained using the CWT (a) and proposed ISD (b) method, respectively.

Code availability section

Name of the code/library: seismic-reservoir-prediction.

Contact: niewenliang@sanxiau.edu.cn.

Hardware requirements: Intel (R) Core (TM) i3-12300 3.50 GHz, 16.0 GB RAM.

Program language: Python and Matlab. Python for AdaBoost-CNN Algorithm; Matlab for generating T-F maps for DL models.

Software required: The built-in Python library.

Program size: 16.7 Mb.

The source codes are available for downloading at the link: https://github.com/SxNeo/seismic-reservoir-prediction/ …

Declaration of competing interest

The authors declare that they have no known competing financial interests or personal relationships that could have appeared to influence the work reported in this paper.

Acknowledgments

The authors would like to acknowledge the support of the Natural Science Foundation of Chongqing, China (CSTB2022NSCQ-MSX0294), the National Key Research and Development Program of China (2021YFB3901400), the Doctoral "Through Train" Scientific Research Project of Wanzhou (WZSTC20220138), the Foundation of Intelligent Ecotourism Subject Group of Chongqing Three Gorges University (NO. zhlv20221016), and Open Fund (PLC 20211105) of State Key Laboratory of Oil and Gas Reservoir Geology and Exploitation(Chengdu University of Technology).

Data availability

Data will be made available on request.

References

Adler, A., Araya-Polo, M., Poggio, T., 2021. Deep learning for seismic inverse problems: toward the acceleration of geophysical analysis workflows. IEEE Signal Process. Mag. 38, 89–119.

Ali, A., Sheng-Chang, C., Ali, S.H.J.P., Geophysics, A., 2022. Integration of density-based spatial clustering with noise and continuous wavelet transform for feature extraction from seismic data. Pure Appl. Geophys. 179, 1183–1195.

Alzubaidi, F., Mostaghimi, P., Swietojanski, P., Clark, S.R., Armstrong, R.T., Engineering, 2021. Automated lithology classification from drill core images using convolutional neural networks. J. Petrol. Sci. Eng. 197, 107933.

Bauer, K., Norden, B., Ivanova, A., Stiller, M., Krawczyk, C.M.J.G.P., 2020. Wavelet transform-based seismic facies classification and modelling: application to a geothermal target horizon in the NE German Basin. Geophys. Prospect. 68, 466–482.

Bonar, D.C., Sacchi, M.D., 2010. Complex Spectral Decomposition via Inversion Strategies. Society of Exploration Geophysicists. Society of Exploration Geophysicists, pp. 1408–1412.

Bosch, M., Mukerji, T., Gonzalez, E.F.J.G., 2010. Seismic inversion for reservoir properties combining statistical rock physics and geostatistics: a review. Geophysics 75, 75A165–175A176.

Czako, Z., Sebestyen, G., Hangan, A., 2021. AutomaticAI–A hybrid approach for automatic artificial intelligence algorithm selection and hyperparameter tuning. Expert Syst. Appl. 182, 115225.

Feng, R., Balling, N., Grana, D., Dramsch, J.S., Hansen, T.M., sensing, r., 2021. Bayesian convolutional neural networks for seismic facies classification. IEEE Trans. Geosci. Rem. Sens. 59, 8933–8940.

Freund, Y., Schapire, R.E., sciences, s., 1997. A decision-theoretic generalization of on-line learning and an application to boosting. J. Comput. Syst. Sci. 55, 119–139.

Goyes-Peñafiel, P., Suárez-Rodríguez, L., Correa, C.V., Arguello, H., Sensing, R., 2024. GAN–supervised seismic data reconstruction: an enhanced–learning for improved generalization. IEEE Trans. Geosci. Rem. 64, 1–10.

Grana, D., Azevedo, L., De Figueiredo, L., Connolly, P., Mukerji, T.J.G., 2022. Probabilistic inversion of seismic data for reservoir petrophysical characterization: review and examples. Geophysics 87, M199–M216.

Grana, D., Azevedo, L., Liu, M.J.G., 2020. A comparison of deep machine learning and Monte Carlo methods for facies classification from seismic data. Geophysics 85, WA41–WA52.

Haixiang, G., Yijing, L., Yanan, L., Xiao, L., Jinling, L., 2016. BPSO-Adaboost-KNN ensemble learning algorithm for multi-class imbalanced data classification. Eng. Appl. Artif. Intell. 49, 176–193.

Hameed, K., Chai, D., Rassau, A.J.A.S., 2020. A sample weight and adaboost cnn-based coarse to fine classification of fruit and vegetables at a supermarket self-checkout. Appl. Sci. 10, 8667.

Hastie, T., Rosset, S., Zhu, J., Zou, H.J.S., Interface, i., 2009. Multi-class adaboost. Stat. Interface 2, 349–360.

Imamverdiyev, Y., Sukhostat, L., Engineering, 2019. Lithological facies classification using deep convolutional neural network. J. Petrol. Sci. Eng. 174, 216–228.

Jo, J.H., Ha, W., Sensing, R., 2024. Seismic traveltime tomography using transfer learning. IEEE Trans. Geosci. Rem. Sens.

Jordão, H., Azevedo, L., Sousa, A.J., Soares, A.J.M.G., 2022. Generative adversarial network applied to ore type modeling in complex geological environments. Math. Geosci. 54, 1165–1182.

Karakaya, S., Ogiesoba, O.C., Olariu, C., Bhattacharya, S.J.G., 2024. Generating 3D lithology probability volumes using poststack inversion, probabilistic neural networks, and Bayesian classification—a case study from the mixed carbonate and siliciclastic deposits of the Cisco Group of the Eastern Shelf of the Permian Basin, north-central Texas. Geophysics 89, B131–B146.

Kitzig, M.C., Kepic, A., Kieu, D.T.J.E.G., 2017. Testing cluster analysis on combined petrophysical and geochemical data for rock mass classification. Explor. Geophys. 48, 344–352.
Li, F., Wu, B., Liu, N., Hu, Y., Wu, H.J.I.G., Letters, R.S., 2019. Seismic time–frequency analysis via adaptive mode separation-based wavelet transform. Geosci. Rem. Sens. Lett. IEEE 17, 696–700.
Li, F., Zhou, H., Wang, Z., Wu, X., Sensing, R., 2020. ADDCNN: an attention-based deep dilated convolutional neural network for seismic facies analysis with interpretable spatial–spectral maps. IEEE Trans. Geosci. Rem. Sens. 59, 1733–1744.
Li, G.-h., Zheng, Y., Li, Y., Wu, W., Hong, Y., Zhou, X., 2018. Lithology recognition of multi-sampling points based on deep belief network. Prog. Geophys. 33, 1660–1665.
Lin, J., Li, H., Liu, N., Gao, J., Li, Z.J.I.G., Letters, R.S., 2020. Automatic lithology identification by applying LSTM to logging data: a case study in X tight rock reservoirs. Geosci. Rem. Sens. Lett. IEEE 18, 1361–1365.
Liu, N., He, T., Tian, Y., Wu, B., Gao, J., Xu, Z.J.I., 2020. Common-azimuth seismic data fault analysis using residual UNet. Interpretation 8, SM25–SM37.
Liu, N., Zhang, Y., Lei, Y., Yang, Y., Wang, Z., Gao, J., Jiang, X., Sensing, R., 2022. Seismic sparse time-frequency network with transfer learning. IEEE Trans. Geosci. Rem. Sens. 60, 1–13.
Maged, A., Xie, M., 2023. Recognition of abnormal patterns in industrial processes with variable window size via convolutional neural networks and AdaBoost. J. Intell. Manuf. 34, 1941–1963.
Miele, R., Azevedo, L.J.S.R., 2024. Physics-informed W-Net GAN for the direct stochastic inversion of fullstack seismic data into facies models. Sci. Rep. 14, 5122.
Nie, W., Wen, X., Yang, J., He, J., Lin, K., Yang, L.J.I., 2020. L1–2 minimization for P-and S-impedance inversion. Interpretation 8, T379–T390.
Nie, W., Xiang, F., Li, B., Wen, X., Nie, X.J.A.S., 2021. Prestack seismic inversion via nonconvex L1-2 regularization. Appl. Sci. 11, 12015.
Okeugo, C., Onuoha, K., Ekwe, C., Anyiam, O., Dim, C., Technology, P., 2019. Application of crossplot and prestack seismic-based impedance inversion for discrimination of lithofacies and fluid prediction in an old producing field, Eastern Niger Delta Basin. J. Pet. Explor. Prod. Technol. 9, 97–110.
Pan, L., Gao, J., Yang, Y., Wang, Z., Gao, Z.J.I.G., Letters, R.S., 2023. Automatic seismic lithology interpretation via multiattribute integrated deep learning. Geosci. Rem. Sens. Lett. IEEE 20, 1–5.
Sahoo, S., Jha, M.K.J.H.j., 2017. Pattern recognition in lithology classification: modeling using neural networks, self-organizing maps and genetic algorithms. Hydrogeol. J. 25, 311.
Singh, H., Seol, Y., Myshakin, E.M.J.S.J., 2020. Automated well-log processing and lithology classification by identifying optimal features through unsupervised and supervised machine-learning algorithms. SPE J. 25, 2778–2800.
Taherkhani, A., Cosma, G., McGinnity, T.M.J.N., 2020. AdaBoost-CNN: an adaptive boosting algorithm for convolutional neural networks to classify multi-class imbalanced datasets using transfer learning. Neurocomputing 404, 351–366.
Wang, L., Zhou, H., Chen, H., Wang, Y., Zhang, Y., Sensing, R., 2022. Structure-guided L1-2 minimization for stable multichannel seismic attenuation compensation. IEEE Trans. Geosci. Rem. Sens. 60, 1–9.
Wang, Y., Ma, X., Zhou, H., Chen, Y.J.G.J.I., 2018. L 1− 2 minimization for exact and stable seismic attenuation compensation. Geophys. J. Int. 213, 1629–1646.
Wu, H., Zhang, B., Li, F., Liu, N.J.G., 2019. Semiautomatic first-arrival picking of microseismic events by using the pixel-wise convolutional image segmentation method. Geophysics 84, V143–V155.
Wu, X., Geng, Z., Shi, Y., Pham, N., Fomel, S., Caumon, G.J.G., 2020. Building realistic structure models to train convolutional neural networks for seismic structural interpretation. Geophysics 85, WA27–WA39.
Yin, P., Lou, Y., He, Q., Xin, J., 2015. Minimization of 1-2 for compressed sensing. SIAM J. Sci. Comput. 37, A536–A563.
Yu, S., Ma, J.J.R.o.G., 2021. Deep learning for geophysics: current and future trends. Rev. Geophys. 59, e2021RG000742.
Zeng, L., Ren, W., Shan, L., Huo, F., Meng, F., Engineering, 2022. Lithology spatial distribution prediction based on recurrent neural network with kriging technology. J. Petrol. Sci. Eng. 214, 110538.
Zeng, L., Ren, W., Shan, L.J.N., 2020. Attention-based bidirectional gated recurrent unit neural networks for well logs prediction and lithology identification. Neurocomputing 414, 153–171.
Zhang, G., Wang, Z., Chen, Y.J.G.J.I., 2018. Deep learning for seismic lithology prediction. Geophys. J. Int. 215, 1368–1387.
Zhang, J., Li, J., Chen, X., Li, Y.J.I.G., Letters, R.S., 2020. Seismic lithology/fluid prediction via a hybrid ISD-CNN. Geosci. Rem. Sens. Lett. IEEE 18, 13–17.
Zhang, K., Lin, N., Zhang, D., Zhang, J., Yang, J., Tian, G., Engineering, 2022. Automatic tracking for seismic horizons using convolution feature analysis and optimization algorithm. J. Petrol. Sci. Eng. 208, 109441.
Zhu, Z., Peng, G., Chen, Y., Gao, H.J.N., 2019. A convolutional neural network based on a capsule network with strong generalization for bearing fault diagnosis. Neurocomputing 323, 62–75.